Elsevier Editorial System(tm) for BRAIN STIMULATION

Manuscript Draft

Manuscript Number: BRS-D-18-00082R1

Title: The effects of high-frequency transcranial random noise stimulation (hf-tRNS) on global motion processing: an equivalent noise approach

Article Type: Original Article

Keywords: global motion; high-frequency transcranial random noise stimulation; internal noise; global sampling; directional tuning

Corresponding Author: Mr. Filippo Ghin, MSc

Corresponding Author's Institution: University Of Lincoln

First Author: Filippo Ghin, MSc

Order of Authors: Filippo Ghin, MSc; Andrea Pavan; Adriano Contillo; George Mather

Abstract: Background: High frequency transcranial random noise stimulation (hf-tRNS) facilitates performance in several perceptual and cognitive tasks, however, little is known on the underlying modulatory mechanisms.
Objective: In this study we compared the effects of hf-tRNS to those of anodal and cathodal tDCS in a global motion direction discrimination task. An equivalent noise (EN) paradigm was used to assess how hf-tRNS modulates the mechanisms underlying local and global motion processing.
Method: Motion coherence threshold and slope of the psychometric function were estimated using an 8AFC task in which observers had to discriminate the motion direction of a random dot kinematogram presented either in the left or right visual hemi-field. During the task hf-tRNS, anodal and cathodal tDCS were delivered over the left hMT+. In a subsequent experiment we implemented an EN paradigm in order to investigate the effects of hf-tRNS on the mechanisms involved in visual motion integration (i.e., internal noise and sampling).
Results: hf-tRNS reduced the motion coherence threshold but did not affect the slope of the psychometric function, suggesting no modulation of stimulus discriminability. Anodal and cathodal tDCS did not produce any modulatory effects. EN analysis in the latter experiment found that hf-tRNS modulates sampling but not internal noise, suggesting that hf-tRNS modulates the integration of local motion cues.
Conclusion: hf-tRNS interacts with the output neurons tuned to directions near to the directional signal, incrementing the signal-to-noise ratio and the pooling of local motion cues and thus increasing the sensitivity for global moving stimuli.

To the Editor of *Brain Stimulation*

Dear Editor,

Please find enclosed a revised version of the research *Article* entitled: “The effects of high-frequency transcranial random noise stimulation (hf-tRNS) on global motion processing: an equivalent noise approach”, by Filippo Ghin, Andrea Pavan, Adriano Contillo and George Mather. We have dealt with all the points raised by the Reviewers and we hope that our manuscript is now satisfactory for publication in *Brain Stimulation*.

In order to illustrate to Reviewers the changes made in the manuscript, we highlighted the alterations in yellow.

This manuscript is original, has not been previously published elsewhere and has not been submitted simultaneously for publication elsewhere.

Sincerely,
Filippo Ghin

Response Letter

Reviewer #1: Ghin et al investigated the influence of high frequency transcranial random noise stimulation (hf-tRNS) on visual motion discrimination as tested by different random dot kinematogram tasks. The main finding was that hf-tRNS applied over left MT reduced the coherence threshold in experiment 1 and increased global sampling in experiment 3. As such the study contains an element of an internal replication which is a strong point. Another strong point is that the finding was specific to the left MT and to the stimulation protocol since only random noise stimulation but not anodal or cathodal tDCS caused significant effects.

R: We thank the Reviewer 1 for her/his positive comments and suggestions that helped us to improve our manuscript. To help pinpoint the changes, we highlighted in yellow the alterations made to the manuscript in response to Reviewer 1' suggestions.

Thus, overall this is a good study but I have some additional comments.

1) *First, the discussion lacks a mechanistic explanation why hf-tRNS improves performance. In this regard it has been shown previously by Van der Groen et al (J neurosci 2016) that tRNS might influence neural computation in accordance to the stochastic resonance principle. The basic idea is that random noise can enhance close-to-threshold signals detected by non-linear systems (such as neurons or peripheral receptors that respond according to an all-or-nothing regime). This principle has been demonstrated for simple visual perception but also for visual motion discrimination tasks (Treviño M et al. Front Hum Neurosci. 2016) and there is evidence suggesting that stochastic resonance effects can be achieved by applying noise directly to visual cortex (Van der Groen, J Neurosci 2016; Schwarzkopf et al, J Neurosci 2011). The stochastic resonance mechanism would fit very well to the results reported here (particularly since the participants tracked the coherence threshold, a paradigm that is beautifully suited to evoke stochastic resonance effects) and the authors should consider this potential explanation which would be very much in line with the arguments of the second-last paragraph discussing the improved sampling as indicated by experiment 3.*
   R: We thank the Reviewer for this helpful suggestion. We have now discussed how the stochastic resonance phenomenon might be the mechanism underlying performance improvement with hf-tRNS. We have also cited and discussed the suggested references. Please see pages 18-19 (lines 594-609).

2) *Second, please model the electric field (e.g. with SimNIBS or other software) and report the results for the different stimulation conditions.*
   R: We have now simulated the electric field for different stimulation conditions. Simulations were performed with the Matlab toolbox COMETS (v.2) (COMputation of Electric field due to Transcranial current Stimulation; Lee, Jung, Lee, & Im, 2017), as this toolbox can simulate the local electric field by selecting location and size of the electrodes (16 and 60 cm^2 in our study). The electric field intensity values for hf-tRNS have also been estimated. We have now added a paragraph for the simulated local electric fields (pages 8-11, lines 257-343). We have also added a short comment in the final discussion section (page 16, line 524-532).

3) *Third, Experiment 2A revealed a significant stimulation x hemi-field interaction for the slope, even though this was not confirmed by post-hoc tests. Please discuss this finding more nuanced than in the current version of the manuscript. How can this significant effect/trend be explained? Is this just unspecific noise or potentially a real effect?*
   R: We have now modified the result section for Experiment 2A and addressed this issue, please see page 12, lines 374-381. In Experiment 2A, the hf-tRNS was delivered over the vertex (Cz) and over the left forehead. We selected this electrode montage to control for

unspecific effects of the stimulation. This control condition was selected because it has been shown that, while participants were engaged on a visual task, application of the hf-tRNS over frontal areas did not produce any modulation of the performance (Campana, Camilleri, Moret, Ghin, & Pavan, 2016; van der Groen & Wenderoth, 2016). We argue that the significant interaction for the slope we found in Experiment 2A is the results of unspecific noise. This is also confirmed by the post-hoc analysis which showed no significant difference amongst conditions.

4) *Forth, the authors argue that tDCS can either hyperpolarize or depolarize membrane potentials. However, it is unclear why changing the membrane potential of whole cell ensembles should be beneficial for performance in the 8 AFC task.*
R: We thank the reviewer for his/her comment. We tested the effects of tDCS over the hMT+ using a direction discrimination task. A similar paradigm was also used in previous works (Antal et al., 2004; Battaglini, Noventa, & Casco, 2017). However, differently from Antal et al. (2004) and Battaglini et al. (2017) which used a single interval forced-choice motion direction discrimination task, in Experiment 1 we implemented an 8AFC as it has been suggested that using a higher number of alternatives in a *m*-AFC can reduce the guessing rate and make each trial more informative (Hou, Lesmes, Dorr, & Lu, 2015). Despite the difference in the task used we aimed at testing if a mechanism similar to that proposed by Antal et al. (2004) and Battaglini et al. (2017) could also account for our results on tDCS (anodal an cathodal). Specifically, in the introduction section of the manuscript (page 3, line 96) we reported: "*Antal et al. (2004) found that application of c-tDCS over the hMT+ resulted in improved performance on a motion direction discrimination task involving coherently moving dots (i.e., signal) presented amongst randomly moving dots (i.e., noise). On the other hand, when only coherent motion was presented, motion direction discrimination performance was hindered by c-tDCS and improved by a-tDCS. Recently it has been suggested that, at low levels of signal-to-noise ratio, c-tDCS might selectively suppress the uncorrelated motion, leaving the correlated motion above the threshold, thus enhancing motion direction discrimination. On the other hand, at high levels of signal-to-noise ratio, a-tDCS might selectively improve motion coherence thresholds by increasing the probability of firing in detectors tuned to the coherent motion direction, especially those detectors that in absence of stimulation do not reach the firing threshold due to internal noise (Battaglini et al., 2017)".* However, the results of our Experiment 1 for both anodal and cathodal tDCS did not show any significant modulation of the coherence threshold. As suggested in the final Discussion section, this discrepancy may depend on the different tasks and stimulation protocols used.

Reviewer #2
These are two interesting studies that partially replicate. Please provide more information about the theory for how the t-RNS is changing performance.
R: We thank the Reviewer 2 for the positive comment. We have now added in the final Discussion section a paragraph explaining how hf-tRNS might modulate behavioural performance according to the stochastic resonance phenomenon. Please see pages 18-19, lines 594-609. Please, also see point 1 of Reviewer 1.

References

Antal, A., Nitsche, M. A., Kruse, W., Kincses, T. Z., Hoffmann, K. P., & Paulus, W. (2004). Direct current stimulation over V5 enhances visuomotor coordination by improving motion perception in humans. *Journal of Cognitive Neuroscience*, *16*(4), 521–527. https://doi.org/10.1162/089892904323057263

Battaglini, L., Noventa, S., & Casco, C. (2017). Anodal and cathodal electrical stimulation over V5 improves motion perception by signal enhancement and noise reduction. *Brain Stimulation*, *10*(4), 773–779. https://doi.org/10.1016/j.brs.2017.04.128

Campana, G., Camilleri, R., Moret, B., Ghin, F., & Pavan, A. (2016). Opposite effects of high-and low-frequency transcranial random noise stimulation probed with visual motion adaptation. *Scientific Reports*, *6*. https://doi.org/10.1038/srep38919

Hou, F., Lesmes, L., Dorr, M., & Lu, Z. (2015). Using 10AFC to further improve the efficiency of the quick CSF method Fang Hou, *15*, 1–18. https://doi.org/10.1167/15.9.2.doi

Lee, C., Jung, Y.-J., Lee, S. J., & Im, C.-H. (2017). COMETS2: An advanced MATLAB toolbox for the numerical analysis of electric fields generated by transcranial direct current stimulation. *Journal of Neuroscience Methods*, *277*, 56–62. JOUR. https://doi.org/https://doi.org/10.1016/j.jneumeth.2016.12.008

van der Groen, O., & Wenderoth, N. (2016). Transcranial random noise stimulation of visual cortex: stochastic resonance enhances central mechanisms of perception. *Journal of Neuroscience*, *36*(19), 5289–5298. https://doi.org/10.1523/JNEUROSCI.4519-15.2016

Highlights

- hf-tRNS, anodal and cathodal tDCS were compared on a global motion perception task
- hf-tRNS enhanced sensitivity (low coherence threshold) for global moving stimuli
- hf-tRNS was tested for motion integration mechanisms: *internal noise* and *sampling*
- hf-tRNS increased *sampling* but did not modulate *internal noise*
- hf-tRNS favours integration of local motion cues increasing motion sensitivity

The effects of high-frequency transcranial random noise stimulation (hf-tRNS) on global motion processing: an equivalent noise approach

Filippo Ghin[1,*], Andrea Pavan[1], Adriano Contillo[2] and George Mather[1]

[1]University of Lincoln, School of Psychology, Brayford Wharf East, Lincoln LN5 7AY, United Kingdom

[2]University of Ferrara, Dipartimento di Fisica e Scienze della Terra , Via Saragat 1, 44122 Ferrara, Italy

[*]**Corresponding author**

Filippo Ghin

University of Lincoln

School of Psychology

Brayford Wharf East

Lincoln LN5 7AT

Email: fghin@lincoln.ac.uk

All authors contributed equally to this work

Abstract

Background: High frequency transcranial random noise stimulation (hf-tRNS) facilitates performance in several perceptual and cognitive tasks, however, little is known on the underlying modulatory mechanisms.

Objective: In this study we compared the effects of hf-tRNS to those of anodal and cathodal tDCS in a global motion direction discrimination task. An equivalent noise (EN) paradigm was used to assess how hf-tRNS modulates the mechanisms underlying local and global motion processing.

Method: Motion coherence threshold and slope of the psychometric function were estimated using an 8AFC task in which observers had to discriminate the motion direction of a random dot kinematogram presented either in the left or right visual hemi-field. During the task hf-tRNS, anodal and cathodal tDCS were delivered over the left hMT^{+}. In a subsequent experiment we implemented an EN paradigm in order to investigate the effects of hf-tRNS on the mechanisms involved in visual motion integration (i.e., *internal noise* and *sampling*).

Results: hf-tRNS reduced the motion coherence threshold but did not affect the slope of the psychometric function, suggesting no modulation of stimulus discriminability. Anodal and cathodal tDCS did not produce any modulatory effects. EN analysis in the latter experiment found that hf-tRNS modulates *sampling* but not *internal noise*, suggesting that hf-tRNS modulates the integration of local motion cues.

Conclusion: hf-tRNS interacts with the output neurons tuned to directions near to the directional signal, incrementing the signal-to-noise ratio and the pooling of local motion cues and thus increasing the sensitivity for global moving stimuli.

Keywords: global motion, high-frequency transcranial random noise stimulation, internal noise, global sampling, directional tuning

Introduction

Transcranial electrical stimulation (tES) is a non-invasive brain stimulation technique in which low-voltage electrical current is delivered to specific cortical sites. The general effect of tES is a sub-threshold polarization of cortical neurons responding too weakly to generate an action potential. By changing intrinsic neural excitability, tES can influence the resting membrane potential and postsynaptic activity of cortical neurons [1–3]. One of the earliest tES protocols involved anodal-cathodal transcranial direct current stimulation (tDCS). It has been proposed that anodal tDCS (a-tDCS) induces a depolarization of the resting membrane potential, so increasing the neural firing rate, whereas the general effect of cathodal tDCS (c-tDCS) is to hyperpolarize the resting membrane potential and so produces a decrement in neural firing rate [1]. Transcranial random noise stimulation (tRNS) is a more recent tES technique that involves delivery of random levels of current at random frequencies usually within 0.1-1000 Hz. The tRNS protocol was first used by Terney and colleagues [4] and generally causes higher neural excitability than tDCS regimes [4–7]. It has been demonstrated that short applications of either broad frequency spectrum tRNS, or high-frequency tRNS (hf-tRNS; 101-640 Hz) induce a temporary decrease of the BOLD signal on the motor cortex [8] and on the visual cortex [9]. Additionally, it has been shown that tRNS can enhance learning of complex arithmetic functions [10], decreasing loudness and distress of tinnitus [11] and boost perceptual learning [12,13]. In general, tRNS results in improved behavioural performance across a range of different visual tasks. For instance, it has been demonstrated that hf-tRNS can improve performance in an orientation discrimination task compared to other types of electrical stimulation (including, low-frequency tRNS, a-tDCS and c-tDCS; [12,13]). More recently we found that hf-tRNS delivered bilaterally over the human medio-temporal complex (hMT^+, an ensemble of visual areas important for visual motion processing [14–16]) can significantly decrease the duration of the motion after-effect [17], possibly by restoring motion sensors to a pre-adapted state. Though its facilitatory effects have been shown in different contexts, the effects of hf-tRNS on the visual system and underlying modulatory mechanisms have not yet been investigated.

So far, findings in visual motion perception show that task characteristics and stimulus parameters are primary factors determining how non-invasive brain stimulation interacts with the neural network state. Most importantly, it has been recognised that tES does not simply increase or decrease neural excitability and thus enhances or worsens performance [18]. Antal et al. [19] found that application of c-tDCS over the hMT^+ resulted in improved performance on a motion direction discrimination task involving coherently moving dots (i.e., signal) presented amongst randomly moving dots (i.e., noise). On the other hand, when only coherent motion was presented, motion

direction discrimination performance was hindered by c-tDCS and improved by a-tDCS. Recently it has been suggested that, at low levels of signal-to-noise ratio, c-tDCS might selectively suppress the uncorrelated motion, leaving the correlated motion above the threshold, thus enhancing motion direction discrimination. On the other hand, at high levels of signal-to-noise ratio, a-tDCS might selectively improve motion coherence thresholds by increasing the probability of firing in detectors tuned to the coherent motion direction, especially those detectors that in absence of stimulation do not reach the firing threshold due to internal noise [20].

hf-tRNS is a form of alternating current that does not polarize the neural membrane in the same way as tDCS does, and its effects at the neural level are still debated. In order to investigate the effects of hf-tRNS on the visual system, we used established paradigms for measuring visual motion perception. In particular, we tested the effects of different tES protocols on global motion perception to further our understanding on how tES can affects visual motion integration. In the first experiment we tested the effects of different tES regimes on a global motion direction discrimination task. Specifically, we estimated observers' coherence threshold while stimulating the left hMT^+ with c-tDCS, a-tDCS, hf-tRNS or Sham stimulation. To anticipate, the results showed that hf-tRNS enhances motion direction discrimination (i.e., lower coherence thresholds) in the contralateral visual hemi-field with respect to the stimulation site, whereas no significant modulation was found for c-tDCS and a-tDCS. A series of control experiments confirmed that the modulation of coherence thresholds was specific to the stimulation site and did not depend on non-specific effects of hf-tRNS.

Global motion processing is assumed to involve the integration of local motion signals in high order visual areas such as hMT^+. The modulation of coherence thresholds by hf-tRNS may depend on changes in estimates of the local direction of moving dots, or on how these local motion estimates are pulled together [21]. During the integration of globally moving dots, changes in *internal noise* would affect the precision with which each dot's direction is estimated, whereas changes in *sampling* levels would influence the number of such local estimates that can be averaged and integrated [21]. In order to determine whether hf-tRNS modulates *internal noise* or global *sampling*, we adopted an Equivalent Noise (EN) paradigm in which we manipulated stimulus variability (i.e., external noise) to estimate the amount of *internal noise* and *sampling* [22]. The results showed that hf-tRNS does not modulate *internal noise* but does modulate *sampling*. The results are discussed in terms of the effects of hf-tRNS on the directional bandwidths of motion sensors.

Experiment 1

Methods

Participants

One author (FG) and fifteen naïve participants took part in Experiment 1. Participants were all right handed and had normal or corrected to normal vision acuity. Each participant filled in a questionnaire in order to exclude history of seizure, implanted metal objects, heart problems or any neurological disease. Methods were implemented following the World Medical Association Declaration of Helsinki [23]. The present study was approved by the Ethics Committee of the University of Lincoln. Written informed consent was obtained from each participant prior enrolment in the study and they were paid for their time.

Apparatus

Stimuli were displayed on a 20-inch HP p1230 monitor with a refresh rate of 85 Hz. Stimuli were generated with Matlab PsychToolbox [24,25]. The screen resolution was 1280 x 1024 pixels. Each pixel subtended 1.6 arcmin. The minimum and maximum luminances of the screen were 0.08 and 74.6 cd/m^2 respectively, and the mean luminance was 37.5 cd/m^2. A gamma-corrected lookup table (LUT) was used so that luminance was a linear function of the digital representation of the image.

Stimuli

Stimuli were random dot kinematograms (RDKs) made up by 150 white dots (diameter: 0.12 deg) presented within a circular aperture (diameter: 8 deg, density: 3 dots/deg^2). Dots drifted at a speed of 13.3 deg/s and had a limited lifetime; after 47 ms each dot vanished and was replaced by a new dot at a different randomly selected position within the circular window. Dots appeared asynchronously on the display and had an equal probability of being selected as a signal dot [26,27]. This was implemented to minimize the presence of local "motion streaks" [28] that could provide strong cues for direction discrimination. In addition, moving dots that moved outside the circular window were also replaced by a new dot at a different randomly location within the circular window, thus always maintaining the same density. The duration of the RDK was ~106 ms. A certain percentage of dots were signal dots, and the remaining dots were noise dots. Signal dots were constrained to move along one of the eight cardinal trajectories, whereas noise dots were positioned at new locations, randomly selected within the circular window, on each successive frame of the motion sequence [29]. We employed a brief stimulus duration and limited dot lifetime

to prevent both covert attentional tracking of the stimulus motion direction and eye movements toward the stimuli [30].

Stimulation techniques

Stimulation was delivered by a battery driven stimulator (BrainSTIM, EMS) through a pair of saline–soaked sponge electrodes. The hf-tRNS consisted of an alternating current of 1.5 mA with 0 offset, applied with random frequencies ranging from 100 to 600Hz. The tDCS consisted of a direct current of 1.5 mA. In the Sham condition, stimulation was delivered for 30 sec before the task [31]. The total duration of the stimulation was ~18 min. The active electrode had an area of 16 cm^2 whereas the reference electrodes had an area of 60 cm^2. The current density was maintained well below the safety limits (always below 1 A/m^2; [32]. The active electrode was placed over the left human medio-temporal complex (hMT^+) while the reference electrode was placed over the vertex (i.e., Cz). When the tDCS stimulation was applied, the polarity of the active electrode was anodal in the a-tDCS condition and cathodal in the c-tDCS condition. Figure 1 shows a representation of the stimuli used in the experiment, the different electrode locations and the electrical waves used.

The target area was localized in all observers by using predetermined coordinates: 3 cm dorsal to inion and 5 cm leftward from there for the localization of the hMT^+. This localization technique has been used in previous studies [33–38] and provides a localization that is consistent with fMRI localizers [39].

[Figure 1]

Figure 1. Schematic representation of stimulus, electrode location and current waves for hf-tRNS, Anodal and Cathodal tDCS. (A) hf-tRNS: polarity of electrodes (in purple) for hf-tRNS changes at random intensities and frequencies. (B) Anodal tDCS: anode electrode (in red) over left hMT^+ and cathode electrode (in blue) over Cz. (C) Cathodal tDCS: cathode electrode (in blue) over left hMT^+ and anode electrode (in red) over Cz. The white circular frame surrounding the moving dots is only for demonstrative purposes and was not presented during the experiment. (D, E, F) Representation of the electric current waves for hf-tRNS, Anodal tDCS and Cathodal tDCS, respectively.

Procedure

Observers performed an eight-alternative forced-choice task (8AFC) for motion direction discrimination. Dots were presented either on the left or on the right visual hemi-field (eccentricity:

12 deg). The observers were instructed to fixate the centre of the screen and to respond to the RDK's motion direction. A representation of the display used is shown in Figures 1A-C.

We delivered a-tDCS, c-tDCS, hf-tRNS and Sham stimulation in separate non-consecutive days for a total of four sessions for each participant. The stimulation was delivered during the execution of the task (online stimulation). In each block, two interleaved adaptive staircases (MLP; [40,41]) were used, one tracking the coherence threshold for the left visual hemi-field and the other for the right visual hemi-field. Coherence threshold and slope for the left and right visual hemi-fields were each estimated from five staircases. Observers performed five blocks per stimulation session. Each staircase consisted of 32 trials.

We estimated coherence threshold (corresponding to 70% correct in direction discrimination) and function slope for each visual hemi-field. The right visual hemi-field was contralateral with respect to the active electrode (i.e., the electrode placed in correspondence of the left hMT^+, whereas the left visual hemi-field was ipsilateral with respect to the stimulation site. If any of the tES regimes modulate the observers' performance on the motion coherence task, then we would expect modulation of the coherence threshold and slope for the contralateral visual hemi-field (i.e., the right visual hemi-field). Participants were unaware of the type of stimulation that was applied in each session. In appendix A we reported the operational workflow of the staircase and the computations used to estimate coherence threshold and slope of the psychometric function.

Results

Figure 2 shows the results of Experiment 1. We performed a repeated measures ANOVA on the estimated coherence thresholds with stimulation type (a-tDCS, c-tDCS, hf-tRNS and Sham) and visual hemi-field (left and right) as within-subjects factors. A significant effect of the visual hemi-field ($F_{(1,15)} = 9.253$, $p = 0.008$, $\eta^2_p = 0.38$) was found, but stimulation type did not reach significance ($F_{(3,45)} = 2.689$, $p = 0.58$, $\eta^2_p = 0.152$). However, the ANOVA reported a significant interaction between stimulation type and visual hemi-field ($F_{(3,45)} = 3.036$, $p = 0.039$, $\eta^2_p = 0.168$). Pairwise comparisons with a False Discovery Rate (FDR) at 0.05 [42] reported a significant decrement of the coherence threshold in the right visual hemi-field (i.e., the visual hemi-field contralateral to the stimulation site) when hf-tRNS was delivered over the left hMT^+, compared to the Sham stimulation ($p = 0.01$), a-tDCS ($p = 0.009$) and c-tDCS ($p = 0.009$). No significant differences in coherence thresholds were found between hf-tRNS and the other stimulation techniques in the left visual hemi-field ($p > 0.05$). Moreover, paired-sample t-tests with FDR at 0.05 reported a significant decrement of the coherence thresholds for the right visual hemi-field with respect to the left visual hemi-field ($p < 0.001$), but only for the hf-tRNS condition, demonstrating

that the improvement on the right visual hemi-field was specific for the stimulation of the left hMT^+.

A repeated measure ANOVA was also performed on the slopes, with stimulation type and visual hemi-field as factors. It did not report any significant main effects or interaction: stimulation type ($F_{(3,45)} = 2.320$, $p = 0.09$, $\eta^2_p = 0.134$), visual hemi-field ($F_{(1,15)} = 1.581$, $p = 0.23$, $\eta^2_p = 0.095$), interaction stimulation type x visual hemi-field ($F_{(3,45)} = 0.680$, $p = 0.57$, $\eta^2_p = 0.043$).

[Figure 2]

Figure 2. Results of Experiment 1. (A) Mean coherence thresholds for each stimulation type and for the two visual hemi-fields. (B) Mean slopes. Error bars ±SEM.

Discussion

The results of Experiment 1 showed that when hf-tRNS was delivered over the left hMT^+ motion direction discrimination improved (i.e., lower coherence thresholds), but only when stimuli were presented on the contralateral visual hemi-field with respect to the stimulation site (i.e., the right visual hemi-field), indicating spatial specificity of the stimulation. In addition, hf-tRNS was the only stimulation able to modulate motion coherence thresholds, producing a coherence threshold decrement of 9% with respect to the contralateral visual hemi-field in the Sham condition, and a decrement of 11% with respect to the ipsilateral visual hemi-field when hf-tRNS was delivered. On the other hand, hf-tRNS did not modulate the slope of the psychometric function, suggesting that hf-tRNS does not modulate the discriminability of the global moving pattern.

Experiment 2

In Experiment 2 we controlled for two possible confounds that may have produced the results of Experiment 1. The aim of the first control experiment (Experiment 2A) was to exclude any unspecific effects of hf-tRNS due to the stimulation over Cz. The aim of the second control experiment (Experiment 2B) was to assess whether hf-tRNS selectively improves global motion direction discrimination only when it is applied over the hMT^+ [14–16].

Methods

Stimuli and Procedure

Stimuli and procedure were the same as in Experiment 1. A new sample of twenty-four participants took part to Experiment 2, twelve were assigned to the first control experiment, and the

other half to the second control experiment. Experiment 2 followed the same procedure as in Experiment 1 except that participants performed only two different and non-consecutive stimulation sessions in which either hf-tRNS or Sham stimulation was delivered. In Experiment 2A one electrode was placed over Cz and one on the left forehead. In Experiment 2B one electrode was placed over Cz, whereas the other electrode was placed over the left V1 (i.e., 3 cm dorsal to the inion and 1 cm leftward).

Results

Figure 3 shows the results for Experiment 2. A repeated measures ANOVA on the coherence thresholds with stimulation type (hf-tRNS and Sham) and visual hemi-field (left and right) as factors was performed on both control experiments. For Experiment 2A (i.e., left forehead stimulation), the ANOVA did not report any significant effects or interaction: stimulation type ($F_{(1,11)} = 0.159$, $p = 0.70$, $\eta^2_p = 0.014$), visual hemi-field ($F_{(1,11)} = 0.001$, $p = 0.99$, $\eta^2_p = 0.001$), interaction stimulation x visual hemi-field ($F_{(1,11)} = 0.102$, $p = 0.76$, $\eta^2_p = 0.009$). Similarly, for Experiment 2B (i.e., left V1 stimulation), ANOVA did not report any significant effect or interaction: stimulation type ($F_{(1,11)} = 0.398$, $p = 0.54$, $\eta^2_p = 0.035$), visual hemi-field ($F_{(1,11)} = 0.138$, $p = 0.72$, $\eta^2_p = 0.012$), interaction stimulation type x visual hemi-field ($F_{(1,11)} = 1.052$, $p = 0.33$, $\eta^2_p = 0.087$).

For Experiment 2A, a repeated measures ANOVA performed on the slopes reported no significant effects of stimulation type ($F_{(1,11)} = 0.096$, $p = 0.76$, $\eta^2_p = 0.009$) and visual hemi-field ($F_{(1,11)} = 0.024$, $p = 0.88$, $\eta^2_p = 0.002$), however, the ANOVA reported a significant interaction between stimulation type and visual hemi-field ($F_{(1,11)} = 6.168$, $p = 0.03$, $\eta^2_p = 0.359$). Post-hoc comparisons with FDR at 0.05 did not report any significant difference between left and right visual hemi-fields for hf-tRNS and Sham stimulation ($p > 0.05$). For Experiment 2B, a repeated measures ANOVA on the slopes did not report any significant effect or interaction: stimulation type ($F_{(1,11)} = 0.10$, $p = 0.92$, $\eta^2_p = 0.001$), visual hemi-field ($F_{(1,11)} = 0.021$, $p = 0.89$, $\eta^2_p = 0.002$), interaction stimulation type x visual hemi-field ($F_{(1,11)} = 0.274$, $p = 0.61$, $\eta^2_p = 0.024$).

[Figure 3]

Figure 3. Results of Experiment 2. Panels A and B show mean coherence thresholds and slopes for the left and right visual hemi-fields with electrodes over the left forehead and Cz. Panels C and D

show mean coherence thresholds and slopes for the left and right visual hemi-fields with electrodes over left V1 and Cz. Error bars ±SEM.

Discussion

The results of Experiment 2, confirmed the spatial specificity of the effect of electrical stimulation observed in Experiment 1. The results of Experiment 2 also did not show any modulation of the function slopes, further confirming that hf-tRNS does not modulate the discriminability of global moving stimuli.

Experiment 3

The aim of Experiment 3 was to investigate the neural mechanisms involved in global motion processing that were modulated by online hf-tRNS. In order to do this, we implemented an equivalent noise paradigm (EN) adapted by Barlow [43], Dakin et al. [21], and Tibber et al. [22]. In an EN paradigm, analogous to coherent motion tasks, participants are required to discriminate the motion direction of globally moving dots against some level of noise. However, differently from the classic coherence tasks, in EN directions are drawn from a Gaussian distribution having a specific mean direction and standard deviation. In this case, noise is obtained by increasing the standard deviation of the distribution of motion directions. Therefore, in EN all dots are signal dots but directional noise can be achieved by increasing the standard deviation with respect to the mean direction. Consequently, higher motion sensitivity depends on the ability to integrate all dot directions [22]. The EN paradigm relies on the idea that visual integration is limited by two factors: *internal noise* and *sampling*. For the direction integration of drifting dots *internal noise* would affect the precision of estimating each dot's direction, whereas *sampling* refers to the number of such estimates that can be averaged over [21]. Additionally, this psychophysical procedure allows performance to be parcelled into separate estimates of local and global processing. The aim of Experiment 3 was to assess how hf-tRNS modulates *internal noise* and *sampling* in order to account for the increased motion sensitivity found in Experiment 1.

Methods

Stimuli and Procedure

For the EN analysis, we employed an averaging task similar to that reported in Tibber et al. [22]. Stimuli were the same as used in Experiment 1, apart from the addition of Gaussian direction noise to the signal dots. One of the authors (AP) and a new sample of thirteen participants

underwent hf-tRNS or Sham stimulation. The order of the stimulation type was counterbalanced across participants. The stimulation protocol was the same as used in the previous Experiments. In order to assess how hf-tRNS modulates local and global processing of visual motion information (i.e., *internal noise* and *sampling*), we implemented the efficient version of the EN paradigm employed by Tibber et al. [22]. In the EN tasks, participants judged whether moving dots were, *on average*, drifting clockwise or counter-clockwise of vertical-upward motion. A vertical reference was provided at fixation, by means of a black vertical line (4 deg length, 0.1 deg width) crossing the fixation point. For the EN paradigm, observers performed two staircases [44] in separate sessions: the first staircase controlled a "zero external noise" condition in which the external noise was set to zero (i.e., the standard deviation of the normal distribution of directions was set to zero), and the second staircase a "high external noise" condition (Figure 4). In the "zero external noise" condition, a simple 1 up-1 down staircase tracked the minimum directional offset from vertical, whereas in the "high external noise" condition a 1 up-2 down staircase tracked the maximum level of external noise that could be tolerated by the observer. That is, the staircase tracked the standard deviation of the normal distribution of directions that produced a direction discrimination performance of 70.7%. In this latter condition, the signal level (i.e., the mean of the normal distribution of direction) was either 45° clockwise or 45° counter clockwise [22]. Staircases terminated after 300 trials. For each participant, for each stimulation type (hf-tRNS and Sham), and for each visual hemi-field (left and right) we estimated *internal noise* and *sampling*. All experimental blocks were preceded by 8 practice trials. In addition, for each staircase we inserted eight catch trials in which the standard deviation of the normal distribution of directions was set to zero, i.e., zero noise condition. This was done to ensure that participants' attention was focused and they were not guessing. In appendix B we report the Equivalent Noise analysis and how *internal noise* and *global sampling* estimates were derived.

Results

Figure 4 shows the result of Experiment 3. Data were analysed using Generalised Estimating Equations (GEE;[45]). GEE analysis uses a quasi-likelihood method to estimate regression coefficients (β) and standard errors (SE) with sampling distributions, and can be used to test main effects and interactions between the dependent variable and corresponding predictor variables [46]. GEE can be considered an extension of generalized linear models implementing corrections for the dependency of within subjects repeated measurements, by applying a working correlation matrix.

GEE was used to analyse *internal noise* and *sampling* estimated with the EN analysis and weighted for their uncertainty values as defined in Eq. (B.7) and Eq. (B.8) (see Appendix B).

Weights were entered in the GEE analysis. A Shapiro-Wilk test showed that results for internal noise were not normally distributed ($p = 0.001$) with a positive skewness 1.22 (SE: 0.32), thus a Gamma function and identity link transformation function were used in the GEE models. In the first model, *internal noise* was the dependent variable, and stimulation type (hf-tRNS vs. Sham), visual hemi-field (right vs. left) and interaction between stimulation type and visual hemi-field were the predictors. An exchangeable correlation matrix was chosen as it showed a better fit with respect to independent and unstructured correlation matrices. Correlation matrix was selected based on the Quasi-likelihood Information Criterion (QIC criteria; [47]). Exchangeable correlation matrix is indicated when there is no logical order of the measurements and they are equally correlated within subjects and not necessarily collected over time [48]. However, it should be noted that GEE analysis is assumed to be robust even against the choice of an incorrect correlational structure [49]. No significant effect for any predictor was found (Table 1).

[Table 1]

Table 1: GEE analysis results for *internal noise* estimates. Estimated coefficients, standard error, Wald statistics and *p* values for stimulation type, visual hemi-field and stimulation type x visual hemi-field predictors.

The same GEE model was also applied to analyse *sampling* estimates (Table 2). A Shapiro-Wilk test showed that results for internal noise were not normally distributed ($p < 0.001$) with a positive skewness 1.30 (SE: 0.32). Gamma function and identity link transformation function were used. Stimulation type (hf-tRNS vs. Sham), visual hemi-field (right vs. left) and interaction between stimulation type and visual hemi-field were included as predictors. An exchangeable working correlation matrix was also used. Comparison of parameters is illustrated in Table 2. The analysis reported a significant effect for stimulation type ($\beta = 1.719$, SE = 0.695, $p < 0.02$) and interaction between stimulation type and visual hemi-field ($\beta = -2.126$, SE = 0.613, $p < 0.001$), while visual hemi-field predictor did not reach statistical significance ($\beta = 0.231$, SE = 0.314, $p > 0.05$). Post-hoc comparisons with a FDR at 0.05 reported a significant difference between hf-tRNS and Sham stimulation for the right visual hemi-field ($p = 0.047$), and a significant difference between the right visual hemi-field and the left visual hemi-field when hf-tRNS was applied ($p = 0.019$). No significant differences were found between right and left visual hemi-field for Sham stimulation, between hf-tRNS and Sham when just the left visual hemi-field was considered, between right

visual hemi-field with hf-tRNS and left visual hemi-field with Sham, and between right visual hemi-field with Sham stimulation and left visual hemi-field with hf-tRNS ($p > 0.05$).

[Table 2]

Table 2. GEE analysis for *Sampling*. Estimated coefficients, standard error, Wald statistics and p-value for stimulation type, visual hemi-field and stimulation type x visual hemi-field.

[Figure 4]

Figure 4. Results of Experiment 3. (A) Mean internal noise estimates (in radians) for left and right visual hemi-fields and for Sham and hf-tRNS stimulations. (B) Mean sampling estimate for left and right visual hemi-fields and for Sham and hf-tRNS stimulations. Error bars ±SEM.

Discussion

The results of Experiment 3 showed that when hf-tRNS was delivered over left hMT^+ it did not modulate *internal noise*. On the other hand, we found an effect on *sampling* (i.e., the number of local motion signals that are averaged over) that increased specifically for the stimuli presented in the right visual hemi-field, i.e., the contralateral hemi-field with respect to the stimulation site. Taken together these results suggest that hf-tRNS selectively modulates perceptual integration mechanisms.

General Discussion

In a series of experiments we assessed the effects of hf-tRNS on a visual global motion task and the underlying modulated neural mechanisms. In Experiment 1, we used a motion coherence task in which participants judged the global motion direction of a RDK presented either in the left or right visual hemi-field. The results showed that, compared to Sham stimulation, c-tDCS and a-tDCS, online hf-tRNS dramatically decreased the coherence thresholds for global moving stimuli, suggesting an increased sensitivity for motion direction discrimination. Importantly, this improvement was found only when stimulating the left hMT^+ with stimuli presented in the right visual hemi-field, i.e., the contralateral visual hemi-field with respect to the stimulation site. Though we reported a modulation of motion coherence thresholds, the hf-tRNS did not modulate stimulus discriminability, as the slope of the psychometric function was not influenced by the stimulation type. Contrary to previous results [19,20] we did not find any modulation when a-tDCS and c-tDCS were delivered during the motion coherence task. Battaglini et al. [20] found that depending on the motion coherence level (i.e., the signal-to-noise ratio), anodal and cathodal tDCS can lead to

opposite effects. At a high level of visual noise (i.e., low coherence) MT neurons, which have a broad tuning to motion direction, could also respond to directions different from the optimal one [50]. The authors suggested that c-tDCS might selectively suppress the uncorrelated motion signals leaving correlated signals above the threshold. This inhibitory modulation would sharpen the tuning of the local motion detectors reducing the probability of responses to non-preferred directions. On the contrary, at a low level of visual noise (i.e., high coherence), threshold reduction by a-tDCS might be the consequence of an increased probability of firing in those neurons that are tuned for the target direction, which without stimulation would remain in a subthreshold activation state.

The discrepancy resulting from our tDCS results might be attributed to the difference in the protocols used (i.e., online vs. offline stimulation). In our study the electrical stimulation was online, whereas in Battaglini et al. [20] it was applied prior to the task (offline stimulation). It has been suggested that in tDCS the time of application with respect to the behavioural task can lead to different outcomes [13,51]. The neural effect of online tDCS is to polarize the neural membrane. Such modulation could partially be restrained by compensatory mechanisms promoted to maintain the optimal homeostasis of the system [52]. On the other hand, offline tDCS can induce aftereffects and promote LTP that can modulate performance on the subsequent behavioural task [53–55]. A speculative explanation of the discrepancy we found is that, while in Battaglini et al.'s [20] study observers' post stimulation performance might have benefited from LTP, in our study the same LTP could have not occurred during the execution of the task [13,51,56]. However, further studies are necessary to better investigate the effects of online and offline tDCS on the visual system and the role of aftereffects.

When a Cz-forehead mount was used (Experiment 2A) no significant difference was observed in coherence thresholds and slopes between hf-tRNS and Sham stimulation for both left and right visual hemi-fields, suggesting that the significant modulatory effect found in Experiment 1 was not due to unspecific effects of the stimulation. Furthermore, we hypothesized that the decrement of coherence thresholds for global motion with hf-tRNS depended on the stimulation of the left hMT^{+}, and could not be attributed to the spreading of the current flow over the cortex, also affecting earlier visual areas [19]. This prediction was confirmed by the results of a second control experiment in which we stimulated the left V1 (Experiment 2B). The results showed no significant differences in coherence thresholds and slopes between hf-tRNS and Sham stimulation conditions, and no significant differences between the left and right visual hemi-fields. These results suggest specificity in the effect of hf-tRNS, for both the visual hemi-field stimulated and for cortical networks involved in the processing of global motion.

Classic motion coherence tasks like those used in Experiment 1 and 2 cannot disentangle the mechanisms underlying local and global motion processing [21,57]. In general, observer's performance in a motion discrimination task is not just limited by the visual system's ability to integrate motion cues across time and space (*sampling*), but also by the ability to determine individual dot trajectories and to segregate the dots composing the signal from those drifting in random directions; these latter mechanisms are particularly influenced by *internal noise* [21,22]. In the last experiment, using an Equivalent Noise paradigm, we estimated the amount of *internal noise* and *sampling* associated with our global motion direction discrimination task and assessed how the underlying mechanisms are modulated by hf-tRNS.

The results showed that hf-tRNS did not modulate the amount of *internal noise*. This suggests that the ability of the observers to estimate local cue directions was not affected by hf-tRNS. On the other hand, results indicated that hf-tRNS dramatically increased *sampling*. *Sampling* refers to the number of estimates of single dots' directions that the system can integrate. When hf-tRNS is delivered during a motion coherence task, it might interact with the ongoing neural activity responding to the directional signal, thus enhancing the activity of those neurons whose preferred direction is close to the signal direction. Specifically, hf-tRNS may engage motion detectors whose activity is below threshold and may synchronize their firing through a non-linear amplification of subthreshold neural oscillatory activity [3,12,58,59]. This stimulation-mediated modulation may increment the signal-to-noise ratio at the neural population level, resulting in augmented sensitivity and lower coherence levels of the stimulus. It is also possible to argue that whereas *internal noise* is linked to the selectivity bandwidth for motion direction, determining the uncertainty with which they respond to a specific direction [57] *sampling* is linked to the intensity with which neurons signal a motion direction. hf-tRNS could spare the selectivity bandwidth of the neurons, but increase the reliability of global motion direction signalling. However, more physiological and behavioural studies are required in order to understand the effects of random noise electrical stimulation on neural noise.

In conclusion, our results show that during application of hf-tRNS, motion coherence thresholds decreased, but there was no change in the slope of the psychometric function. Moreover, these effects were specific for the cortical area stimulated (i.e., left hMT^{+}). In addition, an Equivalent Noise analysis found that hf-tRNS does not affect the amount of *internal noise,* but selectively modulates global *sampling* by increasing the number of local motion cues being integrated.

Conflict of interest

The authors declare that they have no competing financial interests.

Acknowledgments

This study was supported by the College of Social Science of the University of Lincoln. We would like to thank Rita Donato and Chiara Milesi for helping with data collection.

References

[1] Nitsche MA, Cohen LG, Wassermann EM, Priori A, Lang N, Antal A, et al. Transcranial direct current stimulation: State of the art 2008. Brain Stimul 2008;1:206–23. doi:10.1016/j.brs.2008.06.004.

[2] Stagg CJ, Best JG, Stephenson MC, O'Shea J, Wylezinska M, Kincses ZT, et al. Polarity-sensitive modulation of cortical neurotransmitters by transcranial stimulation. J Neurosci 2009;29:5202–6. doi:10.1523/JNEUROSCI.4432-08.2009.

[3] Miniussi C, Harris JA, Ruzzoli M. Modelling non-invasive brain stimulation in cognitive neuroscience. Neurosci Biobehav Rev 2013;37:1702–12. doi:10.1016/j.neubiorev.2013.06.014.

[4] Terney D, Chaieb L, Moliadze V, Antal A, Paulus W. Increasing human brain excitability by transcranial high-frequency random noise stimulation. J Neurosci 2008;28:14147–55. doi:10.1523/JNEUROSCI.4248-08.2008.

[5] Chaieb L, Paulus W, Antal A. Evaluating aftereffects of short-duration transcranial random noise stimulation on cortical excitability. Neural Plast 2011;2011. doi:10.1155/2011/105927.

[6] Moliadze V, Fritzsche G, Antal A. Comparing the efficacy of excitatory transcranial stimulation methods measuring motor evoked potentials. Neural Plast 2014;2014:837141. doi:10.1155/2014/837141.

[7] Inukai Y, Saito K, Sasaki R, Tsuiki S, Miyaguchi S, Kojima S, et al. Comparison of three non-invasive transcranial electrical stimulation methods for increasing cortical excitability. Front Hum Neurosci 2016;10:1–7. doi:10.3389/fnhum.2016.00668.

[8] Chaieb L, Kovacs G, Cziraki C, Greenlee M, Paulus W, Antal A. Short-duration transcranial random noise stimulation induces blood oxygenation level dependent response attenuation in the human motor cortex. Exp Brain Res 2009;198:439–44. doi:10.1007/s00221-009-1938-7.

[9] Saiote C, Polanía R, Rosenberger K, Paulus W, Antal A. High-frequency tRNS reduces BOLD activity during visuomotor learning. PLoS One 2013;8:1–8. doi:10.1371/journal.pone.0059669.

[10] Snowball A, Tachtsidis I, Popescu T, Thompson J, Delazer M, Zamarian L, et al. Long-term enhancement of brain function and cognition using cognitive training and brain stimulation. Curr Biol 2013;23:987–92. doi:10.1016/j.cub.2013.04.045.

[11] Vanneste S, Fregni F, De Ridder D. Head-to-head comparison of transcranial random noise stimulation, transcranial AC stimulation, and transcranial DC stimulation for tinnitus. Front Psychiatry 2013;4:31–3. doi:10.3389/fpsyt.2013.00158.

[12] Fertonani A, Pirulli C, Miniussi C. Random noise stimulation improves neuroplasticity in perceptual learning. J Neurosci 2011;31:15416–23. doi:10.1523/JNEUROSCI.2002-11.2011.

[13] Pirulli C, Fertonani A, Miniussi C. The role of timing in the induction of neuromodulation in perceptual learning by transcranial electric stimulation. Brain Stimul 2013;6:683–9. doi:10.1016/j.brs.2012.12.005.

[14] Braddick OJ, O'Brien JMD, Wattam-Bell J, Atkinson J, Hartley T, Turner R. Brain areas sensitive to coherent visual motion. Perception 2001;30:61–72. doi:10.1068/p3048.

[15] Ajina S, Kennard C, Rees G, Bridge H. Motion area V5/MT+ response to global motion in the absence of V1 resembles early visual cortex. Brain 2015;138:164–78. doi:10.1093/brain/awu328.

[16] Händel B, Lutzenberger W, Thier P, Haarmeier T. Opposite dependencies on visual motion coherence in human area MT+ and early visual cortex. Cereb Cortex 2007;17:1542–9. doi:10.1093/cercor/bhl063.

[17] Campana G, Camilleri R, Moret B, Ghin F, Pavan A. Opposite effects of high- and low-frequency transcranial random noise stimulation probed with visual motion adaptation. Sci Rep 2016;6:38919. doi:10.1038/srep38919.

[18] Fertonani A, Miniussi C. Transcranial electrical stimulation: what we know and do not know about mechanisms. Neurosci 2017;23:109–23. doi:10.1177/1073858416631966.

[19] Antal A, Nitsche MA, Kruse W, Kincses TZ, Hoffmann KP, Paulus W. Direct current stimulation over V5 enhances visuomotor coordination by improving motion perception in humans. J Cogn Neurosci 2004;16:521–7. doi:10.1162/089892904323057263.

[20] Battaglini L, Noventa S, Casco C. Anodal and cathodal electrical stimulation over V5 improves motion perception by signal enhancement and noise reduction. Brain Stimul 2017;10:773–9. doi:10.1016/j.brs.2017.04.128.

[21] Dakin SC, Mareschal I, Bex PJ. Local and global limitations on direction integration assessed using equivalent noise analysis. Vision Res 2005;45:3027–49. doi:10.1016/j.visres.2005.07.037.

[22] Tibber MS, Kelly MG, Jansari A, Dakin SC, Shepherd AJ. An inability to exclude visual noise in migraine. Investig Ophthalmol Vis Sci 2014;55:2539–46. doi:10.1167/iovs.14-13877.

[23] Association WM. World medical association declaration of helsinki: Ethical principles for

medical research involving human subjects. JAMA 2013;310:2191–4. doi:10.1001/jama.2013.281053.

[24] Brainard DH. The psychophysics toolbox. Spat Vis 1997;10:433–6. doi:10.1163/156856897X00357.

[25] Pelli DG. The VideoToolbox software for visual psychophysics: transforming numbers into movies. Spat Vis 1997;10:437–42. doi:10.1163/156856897X00366.

[26] Morgan MJ, Ward R. Interocular delay produces depth in subjectively moving noise patterns. Q J Exp Psychol 1980;32:387–95. doi:10.1080/14640748008401833.

[27] Newsome WT, Paré EB. A Selective impairment of motion perception following lesions of the Middle Temporal visual area (MT). J Neurosci 1988;8:2201–11. doi:http://www.ncbi.nlm.nih.gov/pubmed/3385495.

[28] Geisler WS. Motion streaks provide a spatial code for motion direction. Nature 1999;400:65–9. doi:10.1038/21886.

[29] Scase MO, Braddick OJ, Raymond JE. What is noise for the motion system? Vision Res 2000;36:2579–86. doi:10.1016/0042-6989(95)00325-8.

[30] Martinez-Conde S, Macknik SL, Hubel DH. The role of fixational eye movements in visual perception. Nat Rev Neurosci 2004;5:229–40. doi:10.1038/nrn1348.

[31] Gandiga PC, Hummel FC, Cohen LG. Transcranial DC stimulation (tDCS): A tool for double-blind sham-controlled clinical studies in brain stimulation. Clin Neurophysiol 2006;117:845–50. doi:10.1016/j.clinph.2005.12.003.

[32] Poreisz C, Boros K, Antal A, Paulus W. Safety aspects of transcranial direct current stimulation concerning healthy subjects and patients. Brain Res Bull 2007;72:208–14. doi:10.1016/j.brainresbull.2007.01.004.

[33] Campana G, Cowey A, Walsh V. Visual area V5/MT remembers "what" but not "where." Cereb Cortex 2006;16:1766–70. doi:10.1093/cercor/bhj111.

[34] Campana G, Cowey A, Walsh V. Priming of motion direction and area V5/MT: a test of perceptual memory. Cereb Cortex 2002;12:663–9. doi:10.1093/cercor/12.6.663.

[35] Campana G, Maniglia M, Pavan A. Common (and multiple) neural substrates for static and dynamic motion after-effects: A rTMS investigation. Cortex 2013;49:2590–4. doi:10.1016/j.cortex.2013.07.001.

[36] Laycock R, Crewther DP, Fitzgerald PB, Crewther SG. Evidence for fast signals and later processing in human V1/V2 and V5/ MT+: a TMS study of motion perception. J Neurophysiol 2007;1:1253–62. doi:10.1152/jn.00416.2007.

[37] Pascual-Leone A, Tarazona F, Keenan J, Tormos JM, Hamilton R, Catala MD. Transcranial

magnetic stimulation and neuroplasticity. Neuropsychologia 1998;37:207–17. doi:10.1016/S0028-3932(98)00095-5.

[38] Pavan A, Alexander I, Campana G, Cowey A. Detection of first- and second-order coherent motion in blindsight. Exp Brain Res 2011;214:261–71. doi:10.1007/s00221-011-2828-3.

[39] Thompson B, Aaen-Stockdale C, Koski L, Hess RF. A double dissociation between striate and extrastriate visual cortex for pattern motion perception revealed using rTMS. Hum Brain Mapp 2009;30:3115–26. doi:10.1002/hbm.20736.

[40] Grassi M, Soranzo A. MLP: A MATLAB toolbox for rapid and reliable auditory threshold estimation. Behav Res Methods 2009;41:20–8. doi:10.3758/BRM.41.1.20.

[41] Green DM. A maximum- likelihood method for estimating thresholds in a yes–no task. J Acoust Soc Am 1993;93:2096–105. doi:10.1121/1.406696.

[42] Benjamini Y, Hochberg Y. Controlling the false discovery rate: a practical and powerful approach to multiple testing. J R Staiticatal Soc 1995;57:289–300. doi:http://www.jstor.org/stable/2346101.

[43] Barlow HB. Retinal noise and absolute threshold. J Opt Soc Am 1956;46:634–9. doi:10.1364/JOSA.46.000634.

[44] Levitt H. Transformed up/down methods in psychoacoustics. J Acoust Soc Am 1971;49:467–77. doi:10.1121/1.1912375.

[45] Liang K-Y, Zeger SL. Longitudinal data analysis using generalized linear models. Biometrika 1986;73:13–22. doi:10.1093/biomet/73.1.13.

[46] Ballinger GA. Using generalized estimating equations for longitudinal data analysis. Organ Res Methods 2004;7:127–50. doi:10.1177/1094428104263672.

[47] Pan W. Akaike's information criterion in generalized estimating equations. Biometrics 2001;57:120–5. doi:10.1111/j.0006-341X.2001.00120.x.

[48] Horton NJ, Lipsitz SR. Review of software to fit generalized estimating equation regression models. Am Stat 1999;53:160–9. doi:10.2307/2685737.

[49] Ghisletta P, Spini D. An introduction to generalized estimating equations and an application to assess selectivity effects in a longitudinal study on very old individuals. J Educ Behav Stat 2004;29:421–37. doi:10.3102/10769986029004421.

[50] Albright TD. Direction and orientation selectivity of neurons in visual area MT of the macaque. J Neurophysiol 1984;52:1106 LP-1130.

[51] Pirulli C, Fertonani A, Miniussi C. Is neural hyperpolarization by cathodal stimulation always detrimental at the behavioral level? Front Behav Neurosci 2014;8:1–10. doi:10.3389/fnbeh.2014.00226.

[52] Abraham WC. Metaplasticity: tuning synapses and networks for plasticity. Nat Rev Neurosci 2008;9:387.

[53] Nitsche MA, Fricke K, Henschke U, Schlitterlau A, Liebetanz D, Lang N, et al. Pharmacological modulation of cortical excitability shifts induced by transcranial direct current stimulation in humans. J Physiol 2003;553:293–301. doi:10.1113/jphysiol.2003.049916.

[54] Nitsche MA, Grundey J, Liebetanz D, Lang N, Tergau F, Paulus W. Catecholaminergic consolidation of motor cortical neuroplasticity in humans. Cereb Cortex 2004;14:1240–5. doi:10.1093/cercor/bhh085.

[55] Nitsche MA, Liebetanz D, Schlitterlau A, Henschke U, Fricke K, Frommann K, et al. GABAergic modulation of DC stimulation-induced motor cortex excitability shifts in humans. Eur J Neurosci 2004;19:2720–6. doi:10.1111/j.0953-816X.2004.03398.x.

[56] Antal A, Chaieb L, Cziraki C, Paulus W, Greenlee MW. Cathodal stimulation of human MT+ leads to elevated fMRI signal: A tDCS-fMRI study. Restor Neurol Neurosci 2012;30:255–63. doi:10.3233/RNN-2012-110208.

[57] Manning C, Dakin SC, Tibber MS, Pellicano E. Averaging, not internal noise, limits the development of coherent motion processing. Dev Cogn Neurosci 2014;10:44–56. doi:10.1016/j.dcn.2014.07.004.

[58] Bikson M, Inoue M, Akiyama H, Deans JK, Fox JE, Miyakawa H, et al. Effects of uniform extracellular DC electric fields on excitability in rat hippocampal slices *in vitro*. J Physiol 2004;557:175–90. doi:10.1113/jphysiol.2003.055772.

[59] Ward LM. Physics of neural synchronisation mediated by stochastic resonance. Contemp Phys 2009;50:563–74. doi:10.1080/00107510902879246.

Appendix A

Estimation of coherence threshold and slope from MLP

The operational flow of the staircase to estimate coherence threshold and slope of the psychometric function consisted in acquiring and storing the subject response to the *n*-th trial, selecting the psychometric function maximizing the likelihood of the first *n* trials, estimating the corresponding coherence threshold and presenting it as stimulus for the (*n*+1)-th trial. The estimate subsequent to the last trial was the output of the staircase [40]. The logistic function was used as psychometric function:

$$p(x) = \gamma + \frac{1-\gamma}{1+exp(-\beta(x-\alpha))} \quad \text{Eq. (A.1)}$$

whose slope parameter β was fixed to 1/2, while the midpoint α and the baseline γ were varied to maximize the likelihood. The rationale for such choice was to focus on the position of the threshold on the coherence axis, suppressing the further degree of freedom associated to the growth rate of the psychometric function. However, for the sake of completeness, we also extracted the information about the slope. In order to do this, we made use of a custom best fit routine based on a Metropolis-Hastings algorithm, exploring the parameter space of the logistic function. The algorithm randomly selected a starting point in the parameter space $\{\alpha, \beta, \gamma\}$ and computed the corresponding total likelihood:

$$l_{TOT} = \sum_n ln\,[R_n + (-1)^{R_n} p(x_n)] \quad \text{Eq. (A.2)}$$

over the whole staircase. Here x_n is the coherence of the *n*-th trial, while R_n indicates the corresponding subject response (1 for correct, 0 for wrong). Thereafter, during each iteration of the Metropolis-Hastings, it performed a random step in the parameter space, computed the corresponding total likelihood and compared it to the one of the starting point. If the new likelihood was higher, the algorithm replaced the starting point with the new point, thus accepting the step. Otherwise, the step was rejected. Approximately 150k iterations were performed for each staircase, and the logistic function corresponding to the highest likelihood was returned as the best fitting

curve. Using the best fit parameters, it was possible to compute an estimate for the coherence threshold T_c as the inverse logistic function

$$T_c = \alpha - \frac{1}{\beta} ln \left[\frac{1-\gamma}{p_t-\gamma} - 1 \right] \quad \text{Eq. (A.3)}$$

p_t being the 70% accuracy value acquired by the psychometric function in correspondence of the coherence threshold.

Appendix B

Equivalent Noise Analysis

The core of the Equivalent Noise (EN) parameterisation, as introduced in Dakin et al. [21], consists in describing the total amount of uncertainty in the perception of the stimulus σ_{obs} as the quadratic sum of two independent components:

$$\sigma_{obs}^2 = \frac{\sigma_{\text{int}}^2 + \sigma_{ext}^2}{\eta_{samp}} \quad \text{Eq. (B.1)}$$

The first component σ_{ext} is related to the noise carried by the stimulus (i.e., external noise). The second component σ_{int} encodes the uncertainty that is intrinsic to the observer (i.e., *internal noise*). The sum is rescaled by a factor η_{samp} representing the effective number of simultaneous *sampling*s that are performed on the stimulus by the observer (i.e., *sampling*). While the external noise σ_{ext} and the observed noise σ_{obs} are directly measurable, the *internal noise* σ_{int} and the number of *sampling*s η_{samp} must be computed through Eq. (B.1), thus providing an effective characterisation of the observer.

As aforementioned, and based on Tibber et al. [22], the characterisation was performed through two independent measurements, respectively at *high external noise* and at *zero external noise*. The *high external noise* data point was the average of the last half of reversals of each 1 up-2 down staircase: σ_{obs} was identically equal to 45° ($\pi/4$ radians), while σ_{ext} was the external noise corresponding to an observer accuracy of 70.7% in motion direction discrimination (Figure B.1). The error associated to the measure was the standard deviation of the considered reversals. Regarding the *zero external noise* point, the staircase entries were divided into bins of 0.5° ($8.73 \cdot 10^{-3}$ radians) width. The clockwise rate of non-empty bins, defined as the ratio between the number of clockwise responses and the total number of trials pertaining to each bin, was fitted against a cumulative Gaussian function:

$$CG(\theta) = \frac{1}{2}\left[\mathrm{erf}\left(\frac{\theta-\theta_0}{\sqrt{2}s}\right) - \mathrm{erf}\left(\frac{\pi/2-\theta_0}{\sqrt{2}s}\right)\right] \quad \text{Eq. (B.2)}$$

the angle θ_0 corresponds to the 50% clockwise rate (i.e., the subjective vertical direction), while *s* is the standard deviation of the original Gaussian and encodes the slope of the cumulative function. The fitted function was used to compute the angle corresponding to 70.7% clockwise rate, which was defined as σ_{obs} corresponding to vanishing σ_{ext}. The standard error associated to the observed noise was computed by propagating the fit uncertainties.

[Figure B.1]

Figure B.1. Representation of the Equivalent Noise function (solid black line). The EN function is constrained by two threshold values: the "zero external noise" threshold, which represents the minimum directional offset from vertical that can be discriminated with no external noise, and the "high external noise" threshold, which represents the maximum level of noise (i.e., the directional standard deviation of the normal distribution of directions) that can be tolerated for a large directional offset.

Before computing the EN parameters, there is an important detail that is worth to point out, related to the periodic nature of motion directions. The actual amount of external noise σ_{ext} differs from the standard deviation of the stimulus distribution (σ_{noise}), due to the wrapping generated by the periodicity of directions. The issue had already been pointed out by Dakin et al. [21], whose solution made use of a simulated observer (based on Monte Carlo simulations) to extract the best fitting values of σ_{int} and η_{samp}. However, we used a different approach. A wrapped normal distribution of given standard deviation σ_{noise} is restricted to a 360° (2π radians) interval centred in the mean orientation. Within such interval, the distribution resembles a non-wrapped distribution as long as $\sigma_{noise} \ll 180°$ (π radians) (see Figure B.2A). For larger values, the superposition of the Gaussian tails forces the wrapped distribution to acquire non-zero values in correspondence to the interval boundaries (see Figure B.2B and B.2C).

[Figure B.2]

Figure B.2. (A) Plot of Gaussian (blue) and wrapped Gaussian (yellow) distributions when σ_{noise} is 45° ($\pi/4$ radians). The extremes of the plot represent $\pm 3\pi$. (B) Plot of Gaussian (blue) and wrapped Gaussian (yellow) distributions when σ_{noise} is 90° ($\pi/2$ radians). (C) Plot of Gaussian (blue) and wrapped Gaussian (yellow) distributions when σ_{noise} is 135° ($3\pi/4$ radians). Consider the first two valleys in the interval $\pm\pi$, increasing σ_{noise} the tails of the wrapped Gaussian distribution overlap and this generates an increase of the tails (panel B) and then of the whole distribution (panel C). Besides, the wrapped Gaussian distribution widens.

Our correction consisted in generating a random set of points following a wrapped distribution of standard deviation σ_{noise} and fitting it with a non-wrapped Gaussian, whose standard deviation was then identified as the "effective width" of the distribution, i.e., the external noise σ_{ext}. By iterating the procedure for a uniform distribution of σ_{noise} in the interval $(0, \pi)$ and fitting the resulting points, we ended up with a relation between the "bare" deviation σ_{noise} and the effective σ_{ext}. As it can be seen in Figure B.3, such relation is robustly linear for small σ_{noise} values, departing from the $\sigma_{ext} = \sigma_{noise}$ line as $\sigma_{noise} \sim 90°$ ($\pi/2$ radians). Afterwards, σ_{ext} grows quickly, exceeding 360° (2π radians) (no perceivable preferred direction) as $\sigma_{noise} \simeq 156°$ (2.72 radians). For obvious reasons, it was only necessary to apply this wrapping correction to the high noise data point.

[Figure B.3]

Figure B.3. Relation between σ_{noise} and σ_{ext} (in radians). Blue points indicate the uniform distribution of σ_{noise} fitted with a generalised hyperbolic function (solid red line). The $\sigma_{ext} = \sigma_{noise}$ line, from which the fitted curve departs at $\sigma_{noise} \sim 90°$, is depicted as well (dashed red line). Dotted black lines indicate the position of the point corresponding to $\sigma_{noise} = 156°$ (2.72 radians) and $\sigma_{ext} = 360°$ (2π radians) (no perceivable preferred direction).

Since the two data points lied in two separate regimes, it was possible to further simplify the computation of the EN parameters. First of all, assuming $\sigma_{ext} \gg \sigma_{\text{int}}$ for the high noise data point, Equation B.1 becomes:

$$\sigma_{obs}^2 \simeq \frac{\sigma_{ext}^2}{\eta_{samp}} \qquad \text{Eq. (B.3)}$$

from which it was possible to retrieve the effective *sampling* size η_{samp} associated to each subject:

$$\eta_{samp} \simeq \frac{\sigma_{ext}^2}{\sigma_{obs}^2} \quad \text{Eq. (B.4)}$$

The *internal noise* was then computed from the zero noise data point, for which it holds:

$$\sigma_{obs}^2 = \frac{\sigma_{\text{int}}^2}{\eta_{samp}} \quad \text{Eq. (B.5)}$$

leading to the *internal noise* estimate for each subject:

$$\sigma_{\text{int}} = \sigma_{obs}\sqrt{\eta_{samp}} \quad \text{Eq. (B.6)}$$

Obviously, each pair $\{\eta_{samp}, \sigma_{\text{int}}\}$ comes with uncertainties $\{\delta\eta_{samp}, \delta\sigma_{\text{int}}\}$ that are the simple propagations of the external noise uncertainty $\delta\sigma_{ext}$ of the high external noise point and the observed noise uncertainty $\delta\sigma_{obs}$ of the zero external noise point. The expressions defining such uncertainties are:

$$\delta\eta_{samp} = \frac{2\sigma_{ext}}{\sigma_{obs}^2}\delta\sigma_{ext} \quad \text{Eq. (B.7)}$$

$$\delta\sigma_{\text{int}} = \sqrt{\eta_{samp}(\delta\sigma_{obs})^2 + \frac{\sigma_{obs}^2}{4\eta_{samp}}\left(\delta\eta_{samp}\right)^2} \quad \text{Eq. (B.8)}$$

It is evident that observers with more precise measurements resulted in EN parameters with smaller uncertainties.

The effects of high-frequency transcranial random noise stimulation (hf-tRNS) on global motion processing: an equivalent noise approach

Filippo Ghin[1,*,†], Andrea Pavan[1,†], Adriano Contillo[2,†] and George Mather[1]

[1]University of Lincoln, School of Psychology, Brayford Wharf East, Lincoln LN5 7AY, United Kingdom

[2]University of Ferrara, Dipartimento di Fisica e Scienze della Terra , Via Saragat 1, 44122 Ferrara, Italy

[*]**Corresponding author**

Filippo Ghin

University of Lincoln

School of Psychology

Brayford Wharf East

Lincoln LN5 7AT

Email: fghin@lincoln.ac.uk

[†]Authors with equal contribution

Abstract

Background: High frequency transcranial random noise stimulation (hf-tRNS) facilitates performance in several perceptual and cognitive tasks, however, little is known about the underlying modulatory mechanisms.

Objective: In this study we compared the effects of hf-tRNS to those of anodal and cathodal tDCS in a global motion direction discrimination task. An equivalent noise (EN) paradigm was used to assess how hf-tRNS modulates the mechanisms underlying local and global motion processing.

Method: Motion coherence threshold and slope of the psychometric function were estimated using an 8AFC task in which observers had to discriminate the motion direction of a random dot kinematogram presented either in the left or right visual hemi-field. During the task hf-tRNS, anodal and cathodal tDCS were delivered over the left hMT^{+}. In a subsequent experiment we implemented an EN paradigm in order to investigate the effects of hf-tRNS on the mechanisms involved in visual motion integration (i.e., *internal noise* and *sampling*).

Results: hf-tRNS reduced the motion coherence threshold but did not affect the slope of the psychometric function, suggesting no modulation of stimulus discriminability. Anodal and cathodal tDCS did not produce any modulatory effects. EN analysis in the last experiment found that hf-tRNS modulates *sampling* but not *internal noise*, suggesting that hf-tRNS modulates the integration of local motion cues.

Conclusion: hf-tRNS interacts with the output neurons tuned to directions near to the directional signal, incrementing the signal-to-noise ratio and the pooling of local motion cues and thus increasing the sensitivity for global moving stimuli.

Keywords: global motion, high-frequency transcranial random noise stimulation, internal noise, global sampling, directional tuning

Introduction

Transcranial electrical stimulation (tES) is a non-invasive brain stimulation technique in which low-voltage electrical current is delivered to specific cortical sites. The general effect of tES is a sub-threshold polarization of cortical neurons responding too weakly to generate an action potential. By changing intrinsic neural excitability, tES can influence the resting membrane potential and postsynaptic activity of cortical neurons [1–3]. One of the earliest tES protocols involved anodal-cathodal transcranial direct current stimulation (tDCS). It has been proposed that anodal tDCS (a-tDCS) induces a depolarization of the resting membrane potential, so increasing the neural firing rate, whereas the general effect of cathodal tDCS (c-tDCS) is to hyperpolarize the resting membrane potential and so produce a decrement in neural firing rate [1]. Transcranial random noise stimulation (tRNS) is a more recent tES technique that involves delivery of random levels of current at random frequencies usually within 0.1-1000 Hz. The tRNS protocol was first used by Terney and colleagues [4] and generally causes higher neural excitability than tDCS regimes [4–7]. It has been demonstrated that short applications of either broad frequency spectrum tRNS, or high-frequency tRNS (hf-tRNS; 101-640 Hz) induce a temporary decrease of the BOLD signal on the motor cortex [8] and on the visual cortex [9]. Additionally, it has been shown that tRNS can enhance learning of complex arithmetic functions [10], decrease loudness and distress in tinnitus [11] and boost perceptual learning [12,13]. In general, tRNS results in improved behavioural performance across a range of different visual tasks. For instance, it has been demonstrated that hf-tRNS can improve performance in an orientation discrimination task compared to other types of electrical stimulation (including, low-frequency tRNS, a-tDCS and c-tDCS; [12,13]). More recently we found that hf-tRNS delivered bilaterally over the human medio-temporal complex (hMT^+, an ensemble of visual areas important for visual motion processing [14–16]) can significantly decrease the duration of the motion after-effect [17], possibly by restoring motion sensors to a pre-adapted state. Though its facilitatory effects have been shown in different contexts, the effects of hf-tRNS on the visual system and underlying modulatory mechanisms have not yet been investigated.

So far, findings in visual motion perception show that task characteristics and stimulus parameters are primary factors determining how non-invasive brain stimulation interacts with the neural network state. Most importantly, it has been recognised that tES does not simply increase or decrease neural excitability and thus enhance or worsen performance [18]. Antal et al. [19] found that application of c-tDCS over the hMT^+ resulted in improved performance on a motion direction discrimination task involving coherently moving dots (i.e., signal) presented amongst randomly

moving dots (i.e., noise). On the other hand, when only coherent motion was presented, motion direction discrimination performance was hindered by c-tDCS and improved by a-tDCS. Recently it has been suggested that, at low levels of signal-to-noise ratio, c-tDCS might selectively suppress the uncorrelated motion, leaving the correlated motion above the threshold, thus enhancing motion direction discrimination. On the other hand, at high levels of signal-to-noise ratio, a-tDCS might selectively improve motion coherence thresholds by increasing the probability of firing in detectors tuned to the coherent motion direction, especially those detectors that in absence of stimulation do not reach the firing threshold due to internal noise [20].

hf-tRNS is a form of alternating current that does not polarize the neural membrane in the same way as tDCS does, and its effects at the neural level are still debated. In order to investigate the effects of hf-tRNS on the visual system, we used established paradigms for measuring visual motion perception. In particular, we tested the effects of different tES protocols on global motion perception to further our understanding on how tES can affect visual motion integration. In the first experiment, we tested the effects of different tES regimes on performance in a global motion direction discrimination task. Specifically, we estimated observers' coherence threshold while stimulating the left hMT^+ with c-tDCS, a-tDCS, hf-tRNS or Sham stimulation. To anticipate, the results showed that hf-tRNS enhances motion direction discrimination (i.e., lower coherence thresholds) in the contralateral visual hemi-field with respect to the stimulation site, whereas no significant modulation was found for c-tDCS and a-tDCS. A series of control studies in Experiment 2 confirmed that the modulation of coherence thresholds was specific to the stimulation site and did not depend on non-specific effects of hf-tRNS.

Global motion processing is assumed to involve the integration of local motion signals in high order visual areas such as hMT^+. The modulation of coherence thresholds by hf-tRNS may depend on changes in estimates of the local direction of moving dots, or on how these local motion estimates are pulled together [21]. During the integration of globally moving dots, changes in *internal noise* would affect the precision with which each dot's direction is estimated, whereas changes in *sampling* levels would influence the number of such local estimates that can be averaged and integrated [21]. In order to determine whether hf-tRNS modulates *internal noise* or global *sampling*, we adopted an Equivalent Noise (EN) paradigm in Experiment 3, in which we manipulated stimulus variability (i.e., external noise) to estimate the amount of *internal noise* and *sampling* [22]. The results showed that hf-tRNS does not modulate *internal noise* but does modulate *sampling*. The results are discussed in terms of the effects of hf-tRNS on the directional bandwidths of motion sensors.

Experiment 1

Methods

Participants

One author (FG) and fifteen naïve participants took part in Experiment 1. Participants were all right handed and had normal or corrected to normal visual acuity. Each participant filled in a questionnaire in order to exclude those with a history of seizure, implanted metal objects, heart problems or any neurological disease. Methods were implemented following the World Medical Association Declaration of Helsinki [23]. The present study was approved by the Ethics Committee of the University of Lincoln. Written informed consent was obtained from each participant prior enrolment in the study and they were paid for their time.

Apparatus

Stimuli were displayed on a 20-inch HP p1230 monitor with a refresh rate of 85 Hz. Stimuli were generated with Matlab PsychToolbox [24,25]. The screen resolution was 1280 x 1024 pixels. Each pixel subtended 1.6 arcmin. The minimum and maximum luminances of the screen were 0.08 and 74.6 cd/m^2 respectively, and the mean luminance was 37.5 cd/m^2. A gamma-corrected lookup table (LUT) was used so that luminance was a linear function of the digital representation of the image.

Stimuli

Stimuli were random dot kinematograms (RDKs) made up by 150 white dots (diameter: 0.12 deg) presented within a circular aperture (diameter: 8 deg, density: 3 dots/deg^2). Dots drifted at a speed of 13.3 deg/s and had a limited lifetime; after 47 ms each dot vanished and was replaced by a new dot at a different randomly selected position within the circular window. Dots appeared asynchronously on the display and had an equal probability of being selected as a signal dot [26,27]. This was implemented to minimize the presence of local "motion streaks" [28] that could provide strong cues for direction discrimination. In addition, moving dots that moved outside the circular window were also replaced by a new dot at a different randomly location within the circular window, thus always maintaining the same density. The duration of the RDK was ~106 ms. A certain percentage of dots were signal dots, and the remaining dots were noise dots. Signal dots were constrained to move along one of the eight cardinal trajectories, whereas noise dots were positioned at new locations, randomly selected within the circular window, on each successive frame of the motion sequence [29]. We employed a brief stimulus duration and limited dot lifetime

to prevent both covert attentional tracking of the stimulus motion direction and eye movements toward the stimuli [30].

Stimulation techniques

Stimulation was delivered by a battery driven stimulator (BrainSTIM, EMS) through a pair of saline–soaked sponge electrodes. The hf-tRNS consisted of an alternating current of 1.5 mA with 0 offset, applied with random frequencies ranging from 100 to 600Hz. The tDCS consisted of a direct current of 1.5 mA. In the Sham condition, stimulation was delivered for 30 sec before the task [31]. The total duration of the stimulation was ~18 min. The active electrode had an area of 16 cm^2 whereas the reference electrodes had an area of 60 cm^2. The current density was maintained well below the safety limits (always below 1 A/m^2; [32]). The active electrode was placed over the left human medio-temporal complex (hMT^+) while the reference electrode was placed over the vertex (i.e., Cz). When the tDCS stimulation was applied, the polarity of the active electrode was anodal in the a-tDCS condition and cathodal in the c-tDCS condition. Figure 1 shows a representation of the stimuli used in the experiment, the different electrode locations and the electrical waves used.

The target area was localized in all observers by using predetermined coordinates: 3 cm dorsal to inion and 5 cm leftward from there for the localization of the hMT^+. This localization technique has been used in previous studies [33–38] and provides a localization that is consistent with fMRI localizers [39].

[Figure 1]

Figure 1. Schematic representation of stimulus, electrode location and current waves for hf-tRNS, Anodal and Cathodal tDCS. (A) hf-tRNS: polarity of electrodes (in purple) for hf-tRNS changes at random intensities and frequencies. (B) Anodal tDCS: anode electrode (in red) over left hMT^+ and cathode electrode (in blue) over Cz. (C) Cathodal tDCS: cathode electrode (in blue) over left hMT^+ and anode electrode (in red) over Cz. The white circular frame surrounding the moving dots is only for demonstrative purposes and was not presented during the experiment. (D, E, F) Representation of the electric current waves for hf-tRNS, Anodal tDCS and Cathodal tDCS, respectively.

Procedure

Observers performed an eight-alternative forced-choice task (8AFC) for motion direction discrimination. Dots were presented either in the left or in the right visual hemi-field (eccentricity:

12 deg). The observers were instructed to fixate the centre of the screen and to respond to the RDK's motion direction. A representation of the display used is shown in Figures 1A-C.

We delivered a-tDCS, c-tDCS, hf-tRNS and Sham stimulation in separate non-consecutive days for a total of four sessions for each participant. The stimulation was delivered during the execution of the task (online stimulation). In each block, two interleaved adaptive staircases (MLP; [40,41]) were used, one tracking the coherence threshold for the left visual hemi-field and the other for the right visual hemi-field. Coherence threshold and slope for the left and right visual hemi-fields were each estimated from five staircases. Observers performed five blocks per stimulation session. Each staircase consisted of 32 trials.

We estimated coherence threshold (corresponding to 70% correct in direction discrimination) and function slope for each visual hemi-field. The right visual hemi-field was contralateral with respect to the active electrode (i.e., the electrode placed in correspondence of the left hMT^+, whereas the left visual hemi-field was ipsilateral with respect to the stimulation site. If any of the tES regimes modulate the observers' performance on the motion coherence task, then we would expect modulation of the coherence threshold and slope for the contralateral visual hemi-field (i.e., the right visual hemi-field). Participants were unaware of the type of stimulation that was applied in each session. In appendix A we reported the operational workflow of the staircase and the computations used to estimate coherence threshold and slope of the psychometric function.

Results

Figure 2 shows the results of Experiment 1. We performed a repeated measures ANOVA on the estimated coherence thresholds with stimulation type (a-tDCS, c-tDCS, hf-tRNS and Sham) and visual hemi-field (left and right) as within-subjects factors. A significant effect of the visual hemi-field ($F_{(1,15)} = 9.253$, $p = 0.008$, $\eta^2_p = 0.38$) was found, but stimulation type did not reach significance ($F_{(3,45)} = 2.689$, $p = 0.58$, $\eta^2_p = 0.152$). However, the ANOVA reported a significant interaction between stimulation type and visual hemi-field ($F_{(3,45)} = 3.036$, $p = 0.039$, $\eta^2_p = 0.168$). Pairwise comparisons with a False Discovery Rate (FDR) at 0.05 [42] reported a significant decrement of the coherence threshold in the right visual hemi-field (i.e., the visual hemi-field contralateral to the stimulation site) when hf-tRNS was delivered over the left hMT^+, compared to the Sham stimulation ($p = 0.01$), to a-tDCS ($p = 0.009$) and to c-tDCS ($p = 0.009$). No significant differences in coherence thresholds were found between hf-tRNS and the other stimulation techniques in the left visual hemi-field ($p > 0.05$). Moreover, paired-sample t-tests with FDR at 0.05 reported a significant decrement of the coherence thresholds for the right visual hemi-field with respect to the left visual hemi-field ($p < 0.001$), but only for the hf-tRNS condition, demonstrating

that the improvement on the right visual hemi-field was specific for the stimulation of the left hMT^+.

A repeated measure ANOVA was also performed on the slopes, with stimulation type and visual hemi-field as factors. It did not report any significant main effects or interaction: stimulation type ($F_{(3,45)} = 2.320$, $p = 0.09$, $\eta^2_p = 0.134$), visual hemi-field ($F_{(1,15)} = 1.581$, $p = 0.23$, $\eta^2_p = 0.095$), interaction stimulation type x visual hemi-field ($F_{(3,45)} = 0.680$, $p = 0.57$, $\eta^2_p = 0.043$).

[Figure 2]

Figure 2. Results of Experiment 1. (A) Mean coherence thresholds (%) for each stimulation type and for the two visual hemi-fields. (B) Mean slopes. Error bars ±SEM.

Discussion

The results of Experiment 1 showed that when hf-tRNS was delivered over the left hMT^+ motion direction discrimination improved (i.e., lower coherence thresholds), but only when stimuli were presented on the contralateral visual hemi-field with respect to the stimulation site (i.e., the right visual hemi-field), indicating spatial specificity of the stimulation. In addition, hf-tRNS was the only stimulation able to modulate motion coherence thresholds, producing a coherence threshold decrement of 9% with respect to the contralateral visual hemi-field in the Sham condition, and a decrement of 11% with respect to the ipsilateral visual hemi-field when hf-tRNS was delivered. On the other hand, hf-tRNS did not modulate the slope of the psychometric function, suggesting that hf-tRNS does not modulate the discriminability of the global moving pattern.

Simulation of local electric fields generated by tES

Simulation of local electric fields generated in the visual cortex by anodal and cathodal tDCS was performed using the Matlab toolbox COMETS (v.2) (COMputation of Electric field due to Transcranial current Stimulation [43]). COMETS evaluates the 3D cortical current distributions on a standard human head model using the electrostatic finite element method (FEM). Modelled electrodes had the same size and orientation to those used in the actual experiment. The electrode on the left hMT^+ was placed according to the coordinates in MNI space (in mm) estimated by Plomp et al. [44] for the left MT ROI location, the other electrode was placed on the Vertex. The results showed that continuous current (anodal and cathodal) reached the cortex and that the electric field is focused on the left hMT^+, though there is some spread to other cortical areas (Figure 3).

[Figure 3]

Figure 3. Simulated local electric field generated in the visual cortex by anodal and cathodal tDCS. The peak intensity of the electric field is on the left hMT^+.

The estimated peak electric field was 0.407 V/m for anodal and cathodal tDCS. COMETS only handles continuous current, however, the case of a random current stimulation can be taken into account as a convenient extrapolation of the simple case of (either anodic or cathodic) continuous current, provided that the frequency band of the stimulation lies below a threshold frequency, related to the typical timescale of neural signal propagation. In other words, the rate of variation of the current must be slower than the time needed to propagate through the brain, so that the spatial distribution of the electric field is not affected by the current change. Such threshold frequency can be estimated as the ratio between the typical speed of propagation of electric neural signals (i.e., 80-120 m/s [45]) and the typical linear dimension of the brain (i.e., 0.10-0.15 m [46]). As a consequence, the threshold frequency lies in the order of magnitude of kHz. According to the complex representation of electrical impedance, the electric potential across a circuit:

$$V = |V|e^{\omega t + \phi_V} \quad \text{Eq. (1)}$$

(and therefore the corresponding electric field $E \propto V$) is related to the electric current going through the said circuit:

$$I = |I|e^{\omega t + \phi_I} \quad \text{Eq. (2)}$$

by the complex version of Ohm's law:

$$V = ZI \quad \text{Eq. (3)}$$

In the above equations, vertical brackets indicate amplitudes, ω is the frequency of the signal and ϕ is the phase, t stands for time, and the circuit impedance:

$$Z = R_\omega + jX_\omega \quad \text{Eq. (4)}$$

is a complex number (j is the imaginary unit), whose real part (the resistance R_ω) and imaginary part (the reactance X_ω) both depend on the frequency ω. The complex Ohm's law can be decomposed into two relations, one regarding the amplitudes:

$$|V| = |Z||I| = \sqrt{R_\omega^2 + X_\omega^2}|I| \quad \text{Eq. (5)}$$

and the other regarding the phases:

$$\phi_V = \phi_I + arg(Z) = \phi_I + arctan(X_\omega/R_\omega) \quad \text{Eq. (6)}$$

Being mainly interested in the intensity of the response, we restrict ourselves to Eq. (5). The fact that in the limit $\omega \to 0$, i.e., the case of a continuous current, the standard Ohm's law is retrieved (being $X_0 = 0$ by definition):

$$|V| = R_0|I| \quad \text{Eq. (7)}$$

implies that, for a current of given intensity, the ratio between the potential corresponding to a stimulation frequency $\omega > 0$ and the one corresponding to a stimulation with $\omega = 0$ is:

$$\frac{|V|_\omega}{|V|_0} = \frac{\sqrt{R_\omega^2+X_\omega^2}}{R_0} \quad \text{Eq. (8)}$$

which in turn implies that the electric field is:

$$E_\omega = E_0 \frac{\sqrt{R_\omega^2+X_\omega^2}}{R_0} = E_0 r \quad \text{Eq. (9)}$$

where r is the short form of the ratio in Eq. 9. If we take the value E_0 to be the maximum intensity of the electric field in the case of a continuous current stimulation of given intensity, the above formula allows us to compute the maximum intensity of the electric field in the more general case of a random current of equivalent average intensity, making use of resistance and reactance values pertaining to the materials composing the brain. The values of resistance and reactance at 100 Hz and 600 Hz (i.e., the frequency range of our hf-tRNS stimulation) were extracted from Yang et al. [47] (Figures 6a and 6b), considering their occipital electrode E13. We found that the impedance ratio

of Eq. (9) ranges from $r = 0.476$ (at $\omega = 100Hz$) to $r = 0.177$ (at $\omega = 600Hz$). Therefore, a random stimulation with average current intensity of 1.5 mA will result in a peak electric field $E_0 r$ ranging from 0.192 V/m to 0.072 V/m, depending on the frequency.

As aforementioned, this whole description only holds if the typical frequency of the random stimulation is below the threshold frequency. In fact, in the opposite case, the current varies at a faster rate than the brain can accommodate, resulting in every portion of the brain experiencing a different (and random) stimulation. In this case, it would be impossible to predict the position and magnitude of the peak electric field, even in terms of average intensity.

In conclusion, it is worth stressing that the whole discussion provides only an average estimate of the order of magnitude of the electric field, and no more. On the other hand, such an estimate is sufficient for the purpose of this consistency check.

Experiment 2

In Experiment 2 we controlled for two possible confounds that may have produced the results of Experiment 1. The aim of the first control experiment (Experiment 2A) was to exclude any unspecific effects of hf-tRNS due to the stimulation over Cz. The aim of the second control experiment (Experiment 2B) was to assess whether hf-tRNS selectively improves global motion direction discrimination only when it is applied over the hMT^+ [14–16].

Methods

Stimuli and Procedure

Stimuli and procedure were the same as in Experiment 1. A new sample of twenty-four participants took part to Experiment 2, twelve were assigned to the first control experiment, and the other half to the second control experiment. Experiment 2 followed the same procedure as in Experiment 1 except that participants performed only two different and non-consecutive stimulation sessions in which either hf-tRNS or Sham stimulation was delivered. In Experiment 2A one electrode was placed over Cz and one on the left forehead. In Experiment 2B one electrode was placed over Cz, whereas the other electrode was placed over the left V1 (i.e., 3 cm dorsal to the inion and 1 cm leftward).

Results

Figure 4 shows the results for Experiment 2. A repeated measures ANOVA on the coherence thresholds with stimulation type (hf-tRNS and Sham) and visual hemi-field (left and right) as factors was performed on both control experiments. For Experiment 2A (i.e., left forehead

stimulation), the ANOVA did not report any significant effects or interaction: stimulation type ($F_{(1,11)} = 0.159$, $p = 0.70$, $\eta^2_p = 0.014$), visual hemi-field ($F_{(1,11)} = 0.001$, $p = 0.99$, $\eta^2_p = 0.001$), interaction stimulation x visual hemi-field ($F_{(1,11)} = 0.102$, $p = 0.76$, $\eta^2_p = 0.009$). Similarly, for Experiment 2B (i.e., left V1 stimulation), ANOVA did not report any significant effect or interaction: stimulation type ($F_{(1,11)} = 0.398$, $p = 0.54$, $\eta^2_p = 0.035$), visual hemi-field ($F_{(1,11)} = 0.138$, $p = 0.72$, $\eta^2_p = 0.012$), interaction stimulation type x visual hemi-field ($F_{(1,11)} = 1.052$, $p = 0.33$, $\eta^2_p = 0.087$).

For Experiment 2A, a repeated measures ANOVA performed on the slopes reported no significant effect of the stimulation type ($F_{(1,11)} = 0.096$, $p = 0.76$, $\eta^2_p = 0.009$), no significant effect of the visual hemi field ($F_{(1,11)} = 0.024$, $p = 0.88$, $\eta^2_p = 0.002$), but a significant interaction between stimulation type and visual hemi-field ($F_{(1,11)} = 6.168$, $p = 0.03$, $\eta^2_p = 0.359$). However, since the stimulations (Sham and hf-tRNS) were applied to a region where no effect was expected, and our subsequent post-hoc comparisons with FDR at 0.05 did not report any significant difference between left and right visual hemi-fields for hf-tRNS and Sham stimulations ($p > 0.05$), we ascribed the reported interaction to a stochastic emergence of unspecified noise. For Experiment 2B, a repeated measures ANOVA on the slopes did not report any significant effect or interaction: stimulation type ($F_{(1,11)} = 0.10$, $p = 0.92$, $\eta^2_p = 0.001$), visual hemi-field ($F_{(1,11)} = 0.021$, $p = 0.89$, $\eta^2_p = 0.002$), interaction stimulation type x visual hemi-field ($F_{(1,11)} = 0.274$, $p = 0.61$, $\eta^2_p = 0.024$).

[Figure 4]

Figure 4. Results of Experiment 2. Panels A and B show mean coherence thresholds (%) and slopes for the left and right visual hemi-fields with electrodes over the left forehead and Cz. Panels C and D show mean coherence thresholds and slopes for the left and right visual hemi-fields with electrodes over left V1 and Cz. Error bars ±SEM.

Discussion

The results of Experiment 2, confirmed the spatial specificity of the effect of electrical stimulation observed in Experiment 1. The results of Experiment 2 also did not show any modulation of the function slopes, further confirming that hf-tRNS does not modulate the discriminability of global moving stimuli.

Experiment 3

The aim of Experiment 3 was to investigate the neural mechanisms involved in global motion processing that were modulated by online hf-tRNS. In order to do this, we implemented an equivalent noise paradigm (EN) adapted by Barlow [48], Dakin et al. [21], and Tibber et al. [22]. In an EN paradigm, analogous to coherent motion tasks, participants are required to discriminate the motion direction of globally moving dots against some level of noise. However, differently from the classic coherence tasks, in EN directions are drawn from a Gaussian distribution having a specific mean direction and standard deviation. In this case, noise is obtained by increasing the standard deviation of the distribution of motion directions. Therefore, in EN all dots are signal dots but directional noise can be achieved by increasing the standard deviation with respect to the mean direction. Consequently, higher motion sensitivity depends on the ability to integrate all dot directions [22]. The EN paradigm relies on the idea that visual integration is limited by two factors: *internal noise* and *sampling*. For the direction integration of drifting dots *internal noise* would affect the precision of estimating each dot's direction, whereas *sampling* refers to the number of such estimates that can be averaged over [21]. Additionally, this psychophysical procedure allows performance to be parcelled into separate estimates of local and global processing. The aim of Experiment 3 was to assess how hf-tRNS modulates *internal noise* and *sampling* in order to account for the increased motion sensitivity found in Experiment 1.

Methods

Stimuli and Procedure

For the EN analysis, we employed an averaging task similar to that reported in Tibber et al. [22]. Stimuli were the same as used in Experiment 1, apart from the addition of Gaussian direction noise to the signal dots. One of the authors (AP) and a new sample of thirteen participants underwent hf-tRNS or Sham stimulation. The order of the stimulation type was counterbalanced across participants. The stimulation protocol was the same as used in the previous Experiments. In order to assess how hf-tRNS modulates local and global processing of visual motion information (i.e., *internal noise* and *sampling*), we implemented the efficient version of the EN paradigm employed by Tibber et al. [22]. In the EN tasks, participants judged whether moving dots were, *on average*, drifting clockwise or counter-clockwise of vertical-upward motion. A vertical reference was provided at fixation, by means of a black vertical line (4 deg length, 0.1 deg width) crossing the fixation point. For the EN paradigm, observers performed two staircases [49] in separate sessions: the first staircase controlled a "zero external noise" condition in which the external noise was set to zero (i.e., the standard deviation of the normal distribution of directions was set to zero), and the

second staircase controlled a "high external noise" condition (i.e., the standard deviation of the normal distribution of direction was variable). In the "zero external noise" condition, a simple 1 up-1 down staircase tracked the minimum directional offset from vertical, whereas in the "high external noise" condition a 1 up-2 down staircase tracked the maximum level of external noise that could be tolerated by the observer. That is, the staircase tracked the standard deviation of the normal distribution of directions that produced a direction discrimination performance of 70.7%. In this latter condition, the signal level (i.e., the mean of the normal distribution of direction) was either 45° clockwise or 45° counter clockwise [22]. Staircases terminated after 300 trials. For each participant, for each stimulation type (hf-tRNS and Sham), and for each visual hemi-field (left and right) we estimated *internal noise* and *sampling*. All experimental blocks were preceded by 8 practice trials. In addition, for the "high external noise" condition, we inserted eight catch trials in which the standard deviation of the normal distribution of directions was set to zero, i.e., zero noise condition. This was done to ensure that participants' attention was focused and they were not guessing. In appendix B we report the Equivalent Noise analysis and how *internal noise* and *global sampling* estimates were derived.

Results

Figure 5 shows the result of Experiment 3. Data were analysed using Generalised Estimating Equations (GEE;[50]). GEE analysis uses a quasi-likelihood method to estimate regression coefficients (β) and standard errors (SE) with sampling distributions, and can be used to test main effects and interactions between the dependent variable and corresponding predictor variables [51]. GEE can be considered an extension of generalized linear models implementing corrections for the dependency of within subjects repeated measurements, by applying a working correlation matrix.

GEE was used to analyse *internal noise* and *sampling* estimated with the EN analysis and weighted for their uncertainty values as defined in Eq. (B.7) and Eq. (B.8) (see Appendix B). Weights were entered in the GEE analysis. A Shapiro-Wilk test showed that results for internal noise were not normally distributed ($p = 0.001$) with a positive skewness 1.22 (SE: 0.32), thus a Gamma function and identity link transformation function were used in the GEE models. In the first model, *internal noise* was the dependent variable, and stimulation type (hf-tRNS vs. Sham), visual hemi-field (right vs. left) and interaction between stimulation type and visual hemi-field were the predictors. An exchangeable correlation matrix was chosen as it showed a better fit with respect to independent and unstructured correlation matrices. Correlation matrix was selected based on the Quasi-likelihood Information Criterion (QIC criteria; [52]). Exchangeable correlation matrix is indicated when there is no logical order of the measurements and they are equally correlated within

subjects and not necessarily collected over time [53]. However, it should be noted that GEE analysis is assumed to be robust even against the choice of an incorrect correlational structure [54]. No significant effect for any predictor was found (Table 1).

[Table 1]

Table 1: GEE analysis results for *internal noise* estimates. Estimated coefficients, standard error, Wald statistics and *p* values for stimulation type, visual hemi-field and stimulation type x visual hemi-field predictors.

The same GEE model was also applied to analyse *sampling* estimates (Table 2). A Shapiro-Wilk test showed that results for internal noise were not normally distributed ($p < 0.001$) with a positive skewness 1.30 (SE: 0.32). Gamma function and identity link transformation function were used. Stimulation type (hf-tRNS vs. Sham), visual hemi-field (right vs. left) and interaction between stimulation type and visual hemi-field were included as predictors. An exchangeable working correlation matrix was also used. Comparison of parameters is illustrated in Table 2. The analysis reported a significant effect for stimulation type ($\beta = 1.719$, SE = 0.695, $p < 0.02$) and interaction between stimulation type and visual hemi-field ($\beta = -2.126$, SE = 0.613, $p < 0.001$), while visual hemi-field predictor did not reach statistical significance ($\beta = 0.231$, SE = 0.314, $p > 0.05$). Post-hoc comparisons with a FDR at 0.05 reported a significant difference between hf-tRNS and Sham stimulation for the right visual hemi-field ($p = 0.047$), and a significant difference between the right visual hemi-field and the left visual hemi-field when hf-tRNS was applied ($p = 0.019$). No significant differences were found between right and left visual hemi-field for Sham stimulation, between hf-tRNS and Sham when just the left visual hemi-field was considered, between right visual hemi-field with hf-tRNS and left visual hemi-field with Sham, and between right visual hemi-field with Sham stimulation and left visual hemi-field with hf-tRNS ($p > 0.05$).

[Table 2]

Table 2. GEE analysis results for *Sampling*. Estimated coefficients, standard error, Wald statistics and p-value for stimulation type, visual hemi-field and stimulation type x visual hemi-field predictors.

[Figure 5]

Figure 5. Results of Experiment 3. (A) Mean internal noise estimates (in radians) for left and right visual hemi-fields and for Sham and hf-tRNS stimulations. (B) Mean sampling estimate for left and right visual hemi-fields and for Sham and hf-tRNS stimulations. Error bars ±SEM.

Discussion

The results of Experiment 3 showed that when hf-tRNS was delivered over left hMT^+ it did not modulate *internal noise*. On the other hand, we found an effect on *sampling* (i.e., the number of local motion signals that are averaged over) that increased specifically for the stimuli presented in the right visual hemi-field, i.e., the contralateral hemi-field with respect to the stimulation site. Taken together these results suggest that hf-tRNS selectively modulates perceptual integration mechanisms.

General Discussion

In a series of experiments, we assessed the effects of hf-tRNS on performance in a visual global motion task, and sought to identify the underlying modulated neural mechanisms. In Experiment 1, we used a motion coherence task in which participants judged the global motion direction of a RDK presented either in the left or right visual hemi-field. The results showed that, compared to Sham stimulation, c-tDCS and a-tDCS, online hf-tRNS dramatically decreased the coherence thresholds for global moving stimuli, suggesting an increased sensitivity for motion direction discrimination. Importantly, this improvement was found only when stimulating the left hMT^+ with stimuli presented in the right visual hemi-field, i.e., the contralateral visual hemi-field with respect to the stimulation site. This is compatible with the results of a simulation of the local electric field intensity generated by tDCS. The simulation showed that the continuous current reached the cortex and that the generated electric field is focused on the left hMT^+, though there is some spread to other occipital areas (see Figure 3). Additionally, values of electric field intensity for the hf-tRNS were extrapolated and showed an intensity ranging from 0.192 V/m to 0.072 V/m for the stimulation frequency range considered (i.e., 100 – 600 Hz). However, due to the lack of evidence on how this particular electrical current interacts with the neural signals, we conclude that more physiological studies are necessary to simulate and estimate the local electric field generated by tRNS. Though we reported a modulation of motion coherence thresholds, the hf-tRNS did not modulate stimulus discriminability, as the slope of the psychometric function was not influenced by the stimulation type. Contrary to previous results [19,20] we did not find any modulation when a-tDCS and c-tDCS were delivered during the motion coherence task. Battaglini et al. [20] found that

depending on the motion coherence level (i.e., the signal-to-noise ratio), anodal and cathodal tDCS can lead to opposite effects. At a high level of visual noise (i.e., low coherence) MT neurons, which have a broad tuning to motion direction, could also respond to directions different from the optimal one [55]. The authors suggested that c-tDCS might selectively suppress the uncorrelated motion signals leaving correlated signals above the threshold. This inhibitory modulation would sharpen the tuning of the local motion detectors reducing the probability of responses to non-preferred directions. On the contrary, at a low level of visual noise (i.e., high coherence), threshold reduction by a-tDCS might be the consequence of an increased probability of firing in those neurons that are tuned for the target direction, which without stimulation would remain in a subthreshold activation state.

The discrepancy resulting from our tDCS results might be attributed to the difference in the protocols used (i.e., online vs. offline stimulation). In our study the electrical stimulation was online, whereas in Battaglini et al. [20] it was applied prior to the task (offline stimulation). It has been suggested that in tDCS the time of application with respect to the behavioural task can lead to different outcomes [13,56]. The neural effect of online tDCS is to polarize the neural membrane. Such modulation could partially be restrained by compensatory mechanisms promoted to maintain the optimal homeostasis of the system [57]. On the other hand, offline tDCS can induce aftereffects and promote LTP that can modulate performance on the subsequent behavioural task [58–60]. A speculative explanation of the discrepancy we found is that, while in Battaglini et al.'s [20] study observers' post stimulation performance might have benefited from LTP, in our study the same LTP could have not occurred during the execution of the task [13,56,61]. However, further studies are necessary to better investigate the effects of online and offline tDCS on the visual system and the role of aftereffects.

When a Cz-forehead mount was used (Experiment 2A) no significant difference was observed in coherence thresholds and slopes between hf-tRNS and Sham stimulation for both left and right visual hemi-fields, suggesting that the significant modulatory effect found in Experiment 1 was not due to unspecific effects of the stimulation. Furthermore, we hypothesized that the decrement of coherence thresholds for global motion with hf-tRNS depended on the stimulation of the left hMT^{+}, and could not be attributed to the spreading of the current flow over the cortex, also affecting earlier visual areas [19]. This prediction was confirmed by the results of a second control experiment in which we stimulated the left V1 (Experiment 2B). The results showed no significant differences in coherence thresholds and slopes between hf-tRNS and Sham stimulation conditions, and no significant differences between the left and right visual hemi-fields. These results suggest

specificity in the effect of hf-tRNS, for both the visual hemi-field stimulated and for cortical networks involved in the processing of global motion.

Classic motion coherence tasks like those used in Experiment 1 and 2 cannot disentangle the mechanisms underlying local and global motion processing [21,62]. In general, an observer's performance in a motion discrimination task is not just limited by the visual system's ability to integrate multiple motion cues across time and space (*sampling*), but also by the ability to determine individual dot trajectories and to segregate the dots composing the signal from those drifting in random directions; these latter mechanisms are particularly influenced by *internal noise* [21,22]. In the last experiment, using an Equivalent Noise paradigm, we estimated the amount of *internal noise* and *sampling* associated with our global motion direction discrimination task and assessed how the underlying mechanisms are modulated by hf-tRNS.

The results showed that hf-tRNS did not modulate the amount of *internal noise*. This suggests that the ability of the observers to estimate local cue directions was not affected by hf-tRNS. On the other hand, results indicated that hf-tRNS dramatically increased *sampling*. *Sampling* refers to the number of estimates of single dots' directions that the system can integrate. When hf-tRNS is delivered during a motion coherence task, it might interact with the ongoing neural activity responding to the directional signal, thus enhancing the activity of those neurons whose preferred direction is close to the signal direction. Specifically, hf-tRNS may engage motion detectors whose activity is below threshold and may synchronize their firing through a non-linear amplification of subthreshold neural oscillatory activity [3,12,63,64]. This stimulation-mediated modulation may increment the signal-to-noise ratio at the neural population level, resulting in augmented sensitivity and lower coherence levels of the stimulus. It is also possible to argue that whereas *internal noise* is linked to the selectivity bandwidth for motion direction, determining the uncertainty with which they respond to a specific direction [62] *sampling* is linked to the intensity with which neurons signal a motion direction. hf-tRNS could spare the selectivity bandwidth of the neurons, but increase the reliability of global motion direction signalling. The hf-tRNS-related *sampling* increment could depend on the stochastic resonance phenomenon. Stochastic resonance [65] is a non-linear phenomenon whereby the addition of a random interference (i.e., noise) can enhance the detection of weak stimuli or enhance the information content of a signal. The addition of an optimal amount of noise results in an increment, whereas too much noise results in a deterioration of the performance or information content. hf-tRNS is a random frequency and intensity stimulation that might induce random activity, thus neural noise, in a non-linear system like the brain. The presence of neural noise could enhance the sensitivity of neurons to a weak stimulus [3,66]. Recently, van der Groen and Wenderoth [67] found evidence supporting the stochastic resonance phenomenon.

Specifically, the authors found that the injection of different hf-tRNS intensities modulated detection accuracy of subthreshold stationary stimuli in a stochastic resonance manner. There is also psychophysical evidence that the addition of external visual noise can improve performance in a motion direction discrimination task [68]. The effects of hf-tRNS on the direction discrimination tasks used in our study can be explained within the stochastic resonance framework; that is, the neural noise induced by hf-tRNS could increase the signalling of neurons to a specific motion direction (i.e., *sampling*), and consequently improve the performance. However, more physiological and behavioural studies are required in order to understand the effects of random noise electrical stimulation on neural noise.

In conclusion, our results show that during application of hf-tRNS, motion coherence thresholds decreased, but there was no change in the slope of the psychometric function. Moreover, these effects were specific for the cortical area stimulated (i.e., left hMT^{+}). In addition, an Equivalent Noise analysis found that hf-tRNS does not affect the amount of *internal noise*, but selectively modulates global *sampling* by increasing the number of local motion cues being integrated.

Conflict of interest

The authors declare that they have no competing financial interests.

Acknowledgments

This study was supported by the College of Social Science of the University of Lincoln. We would like to thank Rita Donato and Chiara Milesi for helping with data collection.

References

[1] Nitsche MA, Cohen LG, Wassermann EM, Priori A, Lang N, Antal A, et al. Transcranial direct current stimulation: State of the art 2008. Brain Stimul 2008;1:206–23. doi:10.1016/j.brs.2008.06.004.

[2] Stagg CJ, Best JG, Stephenson MC, O'Shea J, Wylezinska M, Kincses ZT, et al. Polarity-sensitive modulation of cortical neurotransmitters by transcranial stimulation. J Neurosci 2009;29:5202–6. doi:10.1523/JNEUROSCI.4432-08.2009.

[3] Miniussi C, Harris JA, Ruzzoli M. Modelling non-invasive brain stimulation in cognitive neuroscience. Neurosci Biobehav Rev 2013;37:1702–12. doi:10.1016/j.neubiorev.2013.06.014.

[4] Terney D, Chaieb L, Moliadze V, Antal A, Paulus W. Increasing human brain excitability by transcranial high-frequency random noise stimulation. J Neurosci 2008;28:14147–55. doi:10.1523/JNEUROSCI.4248-08.2008.

[5] Chaieb L, Paulus W, Antal A. Evaluating aftereffects of short-duration transcranial random noise stimulation on cortical excitability. Neural Plast 2011;2011. doi:10.1155/2011/105927.

[6] Moliadze V, Fritzsche G, Antal A. Comparing the efficacy of excitatory transcranial stimulation methods measuring motor evoked potentials. Neural Plast 2014;2014:837141. doi:10.1155/2014/837141.

[7] Inukai Y, Saito K, Sasaki R, Tsuiki S, Miyaguchi S, Kojima S, et al. Comparison of three non-invasive transcranial electrical stimulation methods for increasing cortical excitability. Front Hum Neurosci 2016;10:1–7. doi:10.3389/fnhum.2016.00668.

[8] Chaieb L, Kovacs G, Cziraki C, Greenlee M, Paulus W, Antal A. Short-duration transcranial random noise stimulation induces blood oxygenation level dependent response attenuation in the human motor cortex. Exp Brain Res 2009;198:439–44. doi:10.1007/s00221-009-1938-7.

[9] Saiote C, Polanía R, Rosenberger K, Paulus W, Antal A. High-frequency tRNS reduces BOLD activity during visuomotor learning. PLoS One 2013;8:1–8. doi:10.1371/journal.pone.0059669.

[10] Snowball A, Tachtsidis I, Popescu T, Thompson J, Delazer M, Zamarian L, et al. Long-term enhancement of brain function and cognition using cognitive training and brain stimulation.

673 Curr Biol 2013;23:987–92. doi:10.1016/j.cub.2013.04.045.
674 [11] Vanneste S, Fregni F, De Ridder D. Head-to-head comparison of transcranial random noise
675 stimulation, transcranial AC stimulation, and transcranial DC stimulation for tinnitus. Front
676 Psychiatry 2013;4:31–3. doi:10.3389/fpsyt.2013.00158.
677 [12] Fertonani A, Pirulli C, Miniussi C. Random noise stimulation improves neuroplasticity in
678 perceptual learning. J Neurosci 2011;31:15416–23. doi:10.1523/JNEUROSCI.2002-11.2011.
679 [13] Pirulli C, Fertonani A, Miniussi C. The role of timing in the induction of neuromodulation in
680 perceptual learning by transcranial electric stimulation. Brain Stimul 2013;6:683–9.
681 doi:10.1016/j.brs.2012.12.005.
682 [14] Braddick OJ, O'Brien JMD, Wattam-Bell J, Atkinson J, Hartley T, Turner R. Brain areas
683 sensitive to coherent visual motion. Perception 2001;30:61–72. doi:10.1068/p3048.
684 [15] Ajina S, Kennard C, Rees G, Bridge H. Motion area V5/MT+ response to global motion in
685 the absence of V1 resembles early visual cortex. Brain 2015;138:164–78.
686 doi:10.1093/brain/awu328.
687 [16] Händel B, Lutzenberger W, Thier P, Haarmeier T. Opposite dependencies on visual motion
688 coherence in human area MT+ and early visual cortex. Cereb Cortex 2007;17:1542–9.
689 doi:10.1093/cercor/bhl063.
690 [17] Campana G, Camilleri R, Moret B, Ghin F, Pavan A. Opposite effects of high- and low-
691 frequency transcranial random noise stimulation probed with visual motion adaptation. Sci
692 Rep 2016;6:38919. doi:10.1038/srep38919.
693 [18] Fertonani A, Miniussi C. Transcranial electrical stimulation: what we know and do not know
694 about mechanisms. Neurosci 2017;23:109–23. doi:10.1177/1073858416631966.
695 [19] Antal A, Nitsche MA, Kruse W, Kincses TZ, Hoffmann KP, Paulus W. Direct current
696 stimulation over V5 enhances visuomotor coordination by improving motion perception in
697 humans. J Cogn Neurosci 2004;16:521–7. doi:10.1162/089892904323057263.
698 [20] Battaglini L, Noventa S, Casco C. Anodal and cathodal electrical stimulation over V5
699 improves motion perception by signal enhancement and noise reduction. Brain Stimul
700 2017;10:773–9. doi:10.1016/j.brs.2017.04.128.
701 [21] Dakin SC, Mareschal I, Bex PJ. Local and global limitations on direction integration
702 assessed using equivalent noise analysis. Vision Res 2005;45:3027–49.
703 doi:10.1016/j.visres.2005.07.037.
704 [22] Tibber MS, Kelly MG, Jansari A, Dakin SC, Shepherd AJ. An inability to exclude visual
705 noise in migraine. Investig Ophthalmol Vis Sci 2014;55:2539–46. doi:10.1167/iovs.14-
706 13877.

[23] Association WM. World medical association declaration of helsinki: Ethical principles for medical research involving human subjects. JAMA 2013;310:2191–4. doi:10.1001/jama.2013.281053.

[24] Brainard DH. The psychophysics toolbox. Spat Vis 1997;10:433–6. doi:10.1163/156856897X00357.

[25] Pelli DG. The VideoToolbox software for visual psychophysics: transforming numbers into movies. Spat Vis 1997;10:437–42. doi:10.1163/156856897X00366.

[26] Morgan MJ, Ward R. Interocular delay produces depth in subjectively moving noise patterns. Q J Exp Psychol 1980;32:387–95. doi:10.1080/14640748008401833.

[27] Newsome WT, Paré EB. A selective impairment of motion perception following lesions of the Middle Temporal visual area (MT). J Neurosci 1988;8:2201–11. doi:http https://doi.org/10.1523/JNEUROSCI.08-06-02201.1988.

[28] Geisler WS. Motion streaks provide a spatial code for motion direction. Nature 1999;400:65–9. doi:10.1038/21886.

[29] Scase MO, Braddick OJ, Raymond JE. What is noise for the motion system? Vision Res 2000;36:2579–86. doi:10.1016/0042-6989(95)00325-8.

[30] Martinez-Conde S, Macknik SL, Hubel DH. The role of fixational eye movements in visual perception. Nat Rev Neurosci 2004;5:229–40. doi:10.1038/nrn1348.

[31] Gandiga PC, Hummel FC, Cohen LG. Transcranial DC stimulation (tDCS): a tool for double-blind sham-controlled clinical studies in brain stimulation. Clin Neurophysiol 2006;117:845–50. doi:10.1016/j.clinph.2005.12.003.

[32] Poreisz C, Boros K, Antal A, Paulus W. Safety aspects of transcranial direct current stimulation concerning healthy subjects and patients. Brain Res Bull 2007;72:208–14. doi:10.1016/j.brainresbull.2007.01.004.

[33] Campana G, Cowey A, Walsh V. Visual area V5/MT remembers "what" but not "where." Cereb Cortex 2006;16:1766–70. doi:10.1093/cercor/bhj111.

[34] Campana G, Cowey A, Walsh V. Priming of motion direction and area V5/MT: a test of perceptual memory. Cereb Cortex 2002;12:663–9. doi:10.1093/cercor/12.6.663.

[35] Campana G, Maniglia M, Pavan A. Common (and multiple) neural substrates for static and dynamic motion after-effects: A rTMS investigation. Cortex 2013;49:2590–4. doi:10.1016/j.cortex.2013.07.001.

[36] Laycock R, Crewther DP, Fitzgerald PB, Crewther SG. Evidence for fast signals and later processing in human V1/V2 and V5/ MT+: a TMS study of motion perception. J Neurophysiol 2007;1:1253–62. doi:10.1152/jn.00416.2007.

741 [37] Pascual-Leone A, Tarazona F, Keenan J, Tormos JM, Hamilton R, Catala MD. Transcranial
742 magnetic stimulation and neuroplasticity. Neuropsychologia 1998;37:207–17.
743 doi:10.1016/S0028-3932(98)00095-5.
744 [38] Pavan A, Alexander I, Campana G, Cowey A. Detection of first- and second-order coherent
745 motion in blindsight. Exp Brain Res 2011;214:261–71. doi:10.1007/s00221-011-2828-3.
746 [39] Thompson B, Aaen-Stockdale C, Koski L, Hess RF. A double dissociation between striate
747 and extrastriate visual cortex for pattern motion perception revealed using rTMS. Hum Brain
748 Mapp 2009;30:3115–26. doi:10.1002/hbm.20736.
749 [40] Grassi M, Soranzo A. MLP: a MATLAB toolbox for rapid and reliable auditory threshold
750 estimation. Behav Res Methods 2009;41:20–8. doi:10.3758/BRM.41.1.20.
751 [41] Green DM. A maximum- likelihood method for estimating thresholds in a yes–no task. J
752 Acoust Soc Am 1993;93:2096–105. doi:10.1121/1.406696.
753 [42] Benjamini Y, Hochberg Y. Controlling the false discovery rate: a practical and powerful
754 approach to multiple testing. J R Staiticatal Soc 1995;57:289–300.
755 doi:http://www.jstor.org/stable/2346101.
756 [43] Lee C, Jung YJ, Lee SJ, Im CH. COMETS2: an advanced MATLAB toolbox for the
757 numerical analysis of electric fields generated by transcranial direct current stimulation. J
758 Neurosci Methods 2017;277:56–62. doi:10.1016/j.jneumeth.2016.12.008.
759 [44] Plomp G, Hervais-Adelman A, Astolfi L, Michel CM. Early recurrence and ongoing parietal
760 driving during elementary visual processing. Sci Rep 2015;5:18733. doi:10.1038/srep18733.
761 [45] Hartline DK, Colman DR. Rapid conduction and the evolution of giant axons and myelinated
762 fibers. Curr Biol 2007;17:R29–35. doi:10.1016/j.cub.2006.11.042.
763 [46] Lin J, Gandhi O. Computational methods for predicting field intensity. In: Polk C; Postow E,
764 editor. Handb. Biol. Eff. Electromagn. Fields, Boca Raton: CRC Press; 1996, p. 338–97.
765 [47] Yang L, Dai M, Xu C, Zhang G, Li W, Fu F, et al. The frequency spectral properties of
766 electrode-skin contact impedance on human head and its frequency-dependent effects on
767 frequency-difference EIT in stroke detection from 10Hz to 1MHz. PLoS One 2017;12:1–21.
768 doi:10.1371/journal.pone.0170563.
769 [48] Barlow HB. Retinal noise and absolute threshold. J Opt Soc Am 1956;46:634–9.
770 doi:10.1364/JOSA.46.000634.
771 [49] Levitt H. Transformed up/down methods in psychoacoustics. J Acoust Soc Am 1971;49:467–
772 77. doi:10.1121/1.1912375.
773 [50] Liang KY, Zeger SL. Longitudinal data analysis using generalized linear models. Biometrika
774 1986;73:13–22. doi:10.1093/biomet/73.1.13.

[51] Ballinger GA. Using generalized estimating equations for longitudinal data analysis. Organ Res Methods 2004;7:127–50. doi:10.1177/1094428104263672.

[52] Pan W. Akaike's information criterion in generalized estimating equations. Biometrics 2001;57:120–5. doi:10.1111/j.0006-341X.2001.00120.x.

[53] Horton NJ, Lipsitz SR. Review of software to fit generalized estimating equation regression models. Am Stat 1999;53:160–9. doi:10.2307/2685737.

[54] Ghisletta P, Spini D. An introduction to generalized estimating equations and an application to assess selectivity effects in a longitudinal study on very old individuals. J Educ Behav Stat 2004;29:421–37. doi:10.3102/10769986029004421.

[55] Albright TD. Direction and orientation selectivity of neurons in visual area MT of the macaque. J Neurophysiol 1984;52:1106–30.

[56] Pirulli C, Fertonani A, Miniussi C. Is neural hyperpolarization by cathodal stimulation always detrimental at the behavioral level? Front Behav Neurosci 2014;8:1–10. doi:10.3389/fnbeh.2014.00226.

[57] Abraham WC. Metaplasticity: tuning synapses and networks for plasticity. Nat Rev Neurosci 2008;9:387. doi:10.1038/nrn2356.

[58] Nitsche MA, Fricke K, Henschke U, Schlitterlau A, Liebetanz D, Lang N, et al. Pharmacological modulation of cortical excitability shifts induced by transcranial direct current stimulation in humans. J Physiol 2003;553:293–301. doi:10.1113/jphysiol.2003.049916.

[59] Nitsche MA, Grundey J, Liebetanz D, Lang N, Tergau F, Paulus W. Catecholaminergic consolidation of motor cortical neuroplasticity in humans. Cereb Cortex 2004;14:1240–5. doi:10.1093/cercor/bhh085.

[60] Nitsche MA, Liebetanz D, Schlitterlau A, Henschke U, Fricke K, Frommann K, et al. GABAergic modulation of DC stimulation-induced motor cortex excitability shifts in humans. Eur J Neurosci 2004;19:2720–6. doi:10.1111/j.0953-816X.2004.03398.x.

[61] Antal A, Chaieb L, Cziraki C, Paulus W, Greenlee MW. Cathodal stimulation of human MT+ leads to elevated fMRI signal: a tDCS-fMRI study. Restor Neurol Neurosci 2012;30:255–63. doi:10.3233/RNN-2012-110208.

[62] Manning C, Dakin SC, Tibber MS, Pellicano E. Averaging, not internal noise, limits the development of coherent motion processing. Dev Cogn Neurosci 2014;10:44–56. doi:10.1016/j.dcn.2014.07.004.

[63] Bikson M, Inoue M, Akiyama H, Deans JK, Fox JE, Miyakawa H, et al. Effects of uniform extracellular DC electric fields on excitability in rat hippocampal slices *in vitro*. J Physiol

2004;557:175–90. doi:10.1113/jphysiol.2003.055772.
[64] Ward LM. Physics of neural synchronisation mediated by stochastic resonance. Contemp Phys 2009;50:563–74. doi:10.1080/00107510902879246.
[65] Moss F, Ward LM, Sannita WG. Stochastic resonance and sensory information processing: a tutorial and review of application. Clin Neurophysiol 2004;115:267–81. doi:10.1016/j.clinph.2003.09.014.
[66] Schwarzkopf DS, Silvanto J, Rees G. Stochastic resonance effects reveal the neural mechanisms of transcranial magnetic stimulation. J Neurosci 2011;31:3143–7. doi:10.1523/JNEUROSCI.4863-10.2011.
[67] van der Groen O, Wenderoth N. Transcranial random noise stimulation of visual cortex: stochastic resonance enhances central mechanisms of perception. J Neurosci 2016;36:5289–98. doi:10.1523/JNEUROSCI.4519-15.2016.
[68] Treviño M, la Torre-Valdovinos B, Manjarrez E. Noise improves visual motion discrimination via a stochastic resonance-like phenomenon. Front Hum Neurosci 2016;10:572. doi:10.3389/fnhum.2016.00572.

Appendix A

Estimation of coherence threshold and slope from MLP

The operational flow of the staircase to estimate coherence threshold and slope of the psychometric function consisted in acquiring and storing the subject response to the *n*-th trial, selecting the psychometric function maximizing the likelihood of the first *n* trials, estimating the corresponding coherence threshold and presenting it as stimulus for the (*n*+1)-th trial. The estimate subsequent to the last trial was the output of the staircase [40]. The logistic function was used as psychometric function:

$$p(x) = \gamma + \frac{1-\gamma}{1+exp(-\beta(x-\alpha))} \quad \text{Eq. (A.1)}$$

whose slope parameter β was fixed to 1/2, while the midpoint α and the baseline γ were varied to maximize the likelihood. The rationale for such choice was to focus on the position of the threshold on the coherence axis, suppressing the further degree of freedom associated to the growth rate of the psychometric function. However, for the sake of completeness, we also extracted the information about the slope. In order to do this, we made use of a custom best fit routine based on a Metropolis-Hastings algorithm, exploring the parameter space of the logistic function. The algorithm randomly selected a starting point in the parameter space $\{\alpha, \beta, \gamma\}$ and computed the corresponding total likelihood:

$$l_{TOT} = \sum_n ln\,[R_n + (-1)^{R_n} p(x_n)] \quad \text{Eq. (A.2)}$$

over the whole staircase. Here x_n is the coherence of the *n*-th trial, while R_n indicates the corresponding subject response (1 for correct, 0 for wrong). Thereafter, during each iteration of the Metropolis-Hastings, it performed a random step in the parameter space, computed the corresponding total likelihood and compared it to the one of the starting point. If the new likelihood was higher, the algorithm replaced the starting point with the new point, thus accepting the step. Otherwise, the step was rejected. Approximately 150k iterations were performed for each staircase, and the logistic function corresponding to the highest likelihood was returned as the best fitting

curve. Using the best fit parameters, it was possible to compute an estimate for the coherence threshold T_c as the inverse logistic function

$$T_c = \alpha - \frac{1}{\beta} ln \left[\frac{1-\gamma}{p_t-\gamma} - 1 \right] \quad \text{Eq. (A.3)}$$

p_t being the 70% accuracy value acquired by the psychometric function in correspondence of the coherence threshold.

Appendix B

Equivalent Noise Analysis

The core of the Equivalent Noise (EN) parameterisation, as introduced in Dakin et al. [21], consists in describing the total amount of uncertainty in the perception of the stimulus σ_{obs} as the quadratic sum of two independent components:

$$\sigma_{obs}^2 = \frac{\sigma_{\text{int}}^2 + \sigma_{ext}^2}{\eta_{samp}} \quad \text{Eq. (B.1)}$$

The first component σ_{ext} is related to the noise carried by the stimulus (i.e., external noise). The second component σ_{int} encodes the uncertainty that is intrinsic to the observer (i.e., *internal noise*). The sum is rescaled by a factor η_{samp} representing the effective number of simultaneous *sampling*s that are performed on the stimulus by the observer (i.e., *sampling*). While the external noise σ_{ext} and the observed noise σ_{obs} are directly measurable, the *internal noise* σ_{int} and the number of *sampling*s η_{samp} must be computed through Eq. (B.1), thus providing an effective characterisation of the observer.

As aforementioned, and based on Tibber et al. [22], the characterisation was performed through two independent measurements, respectively at *high external noise* and at *zero external noise*. The *high external noise* data point was the average of the last half of reversals of each 1 up-2 down staircase: σ_{obs} was identically equal to 45° (π/4 radians), while σ_{ext} was the external noise corresponding to an observer accuracy of 70.7% in motion direction discrimination (Figure B.1). The error associated to the measure was the standard deviation of the considered reversals. Regarding the *zero external noise* point, the staircase entries were divided into bins of 0.5° ($8.73 \cdot 10^{-3}$ radians) width. The clockwise rate of non-empty bins, defined as the ratio between the number of clockwise responses and the total number of trials pertaining to each bin, was fitted against a cumulative Gaussian function:

$$CG(\theta) = \frac{1}{2}\left[\mathrm{erf}\left(\frac{\theta-\theta_0}{\sqrt{2}s}\right) - \mathrm{erf}\left(\frac{\pi/2-\theta_0}{\sqrt{2}s}\right)\right] \quad \text{Eq. (B.2)}$$

the angle θ_0 corresponds to the 50% clockwise rate (i.e., the subjective vertical direction), while *s* is the standard deviation of the original Gaussian and encodes the slope of the cumulative function. The fitted function was used to compute the angle corresponding to 70.7% clockwise rate, which was defined as σ_{obs} corresponding to vanishing σ_{ext}. The standard error associated to the observed noise was computed by propagating the fit uncertainties.

[Figure B.1]

Figure B.1. Representation of the Equivalent Noise function (solid black line). The EN function is constrained by two threshold values: the "zero external noise" threshold, which represents the minimum directional offset from vertical that can be discriminated with no external noise, and the "high external noise" threshold, which represents the maximum level of noise (i.e., the directional standard deviation of the normal distribution of directions) that can be tolerated for a large directional offset.

Before computing the EN parameters, there is an important detail that is worth to point out, related to the periodic nature of motion directions. The actual amount of external noise σ_{ext} differs from the standard deviation of the stimulus distribution (σ_{noise}), due to the wrapping generated by the periodicity of directions. The issue had already been pointed out by Dakin et al. [21], whose solution made use of a simulated observer (based on Monte Carlo simulations) to extract the best fitting values of σ_{int} and η_{samp}. However, we used a different approach. A wrapped normal distribution of given standard deviation σ_{noise} is restricted to a 360° (2π radians) interval centred in the mean orientation. Within such interval, the distribution resembles a non-wrapped distribution as long as $\sigma_{noise} \ll 180°$ (π radians) (see Figure B.2A). For larger values, the superposition of the Gaussian tails forces the wrapped distribution to acquire non-zero values in correspondence to the interval boundaries (see Figure B.2B and B.2C).

[Figure B.2]

Figure B.2. (A) Plot of Gaussian (blue) and wrapped Gaussian (yellow) distributions when σ_{noise} is 45° (π/4 radians). The extremes of the plot represent ±3π. (B) Plot of Gaussian (blue) and wrapped Gaussian (yellow) distributions when σ_{noise} is 90° (π/2 radians). (C) Plot of Gaussian (blue) and

wrapped Gaussian (yellow) distributions when σ_{noise} is 135° (3π/4 radians). Consider the first two valleys in the interval ±π, increasing σ_{noise} the tails of the wrapped Gaussian distribution overlap and this generates an increase of the tails (panel B) and then of the whole distribution (panel C). Besides, the wrapped Gaussian distribution widens.

Our correction consisted in generating a random set of points following a wrapped distribution of standard deviation σ_{noise} and fitting it with a non-wrapped Gaussian, whose standard deviation was then identified as the "effective width" of the distribution, i.e., the external noise σ_{ext}. By iterating the procedure for a uniform distribution of σ_{noise} in the interval (0, π) and fitting the resulting points, we ended up with a relation between the "bare" deviation σ_{noise} and the effective σ_{ext}. As it can be seen in Figure B.3, such relation is robustly linear for small σ_{noise} values, departing from the $\sigma_{ext} = \sigma_{noise}$ line as $\sigma_{noise} \sim 90°$ ($\pi/2$ radians). Afterwards, σ_{ext} grows quickly, exceeding 360° (2π radians) (no perceivable preferred direction) as $\sigma_{noise} \simeq 156°$ (2.72 radians). For obvious reasons, it was only necessary to apply this wrapping correction to the high noise data point.

[Figure B.3]

Figure B.3. Relation between σ_{noise} and σ_{ext} (in radians). Blue points indicate the uniform distribution of σ_{noise} fitted with a generalised hyperbolic function (solid red line). The $\sigma_{ext} = \sigma_{noise}$ line, from which the fitted curve departs at $\sigma_{noise} \sim 90°$, is depicted as well (dashed red line). Dotted black lines indicate the position of the point corresponding to $\sigma_{noise} = 156°$ (2.72 radians) and $\sigma_{ext} = 360°$ (2π radians) (no perceivable preferred direction).

Since the two data points lied in two separate regimes, it was possible to further simplify the computation of the EN parameters. First of all, assuming $\sigma_{ext} \gg \sigma_{\text{int}}$ for the high noise data point, Equation B.1 becomes:

$$\sigma_{obs}^2 \simeq \frac{\sigma_{ext}^2}{\eta_{samp}} \qquad \text{Eq. (B.3)}$$

from which it was possible to retrieve the effective *sampling* size η_{samp} associated to each subject:

$$\eta_{samp} \simeq \frac{\sigma_{ext}^2}{\sigma_{obs}^2} \qquad \text{Eq. (B.4)}$$

The *internal noise* was then computed from the zero noise data point, for which it holds:

$$\sigma_{obs}^2 = \frac{\sigma_{\text{int}}^2}{\eta_{samp}} \quad \text{Eq. (B.5)}$$

leading to the *internal noise* estimate for each subject:

$$\sigma_{\text{int}} = \sigma_{obs}\sqrt{\eta_{samp}} \quad \text{Eq. (B.6)}$$

Obviously, each pair $\{\eta_{samp}, \sigma_{\text{int}}\}$ comes with uncertainties $\{\delta\eta_{samp}, \delta\sigma_{\text{int}}\}$ that are the simple propagations of the external noise uncertainty $\delta\sigma_{ext}$ of the high external noise point and the observed noise uncertainty $\delta\sigma_{obs}$ of the zero external noise point. The expressions defining such uncertainties are:

$$\delta\eta_{samp} = \frac{2\sigma_{ext}}{\sigma_{obs}^2}\delta\sigma_{ext} \quad \text{Eq. (B.7)}$$

$$\delta\sigma_{\text{int}} = \sqrt{\eta_{samp}(\delta\sigma_{obs})^2 + \frac{\sigma_{obs}^2}{4\eta_{samp}}\left(\delta\eta_{samp}\right)^2} \quad \text{Eq. (B.8)}$$

It is evident that observers with more precise measurements resulted in EN parameters with smaller uncertainties.

Figure 1

Click here to download high resolution image

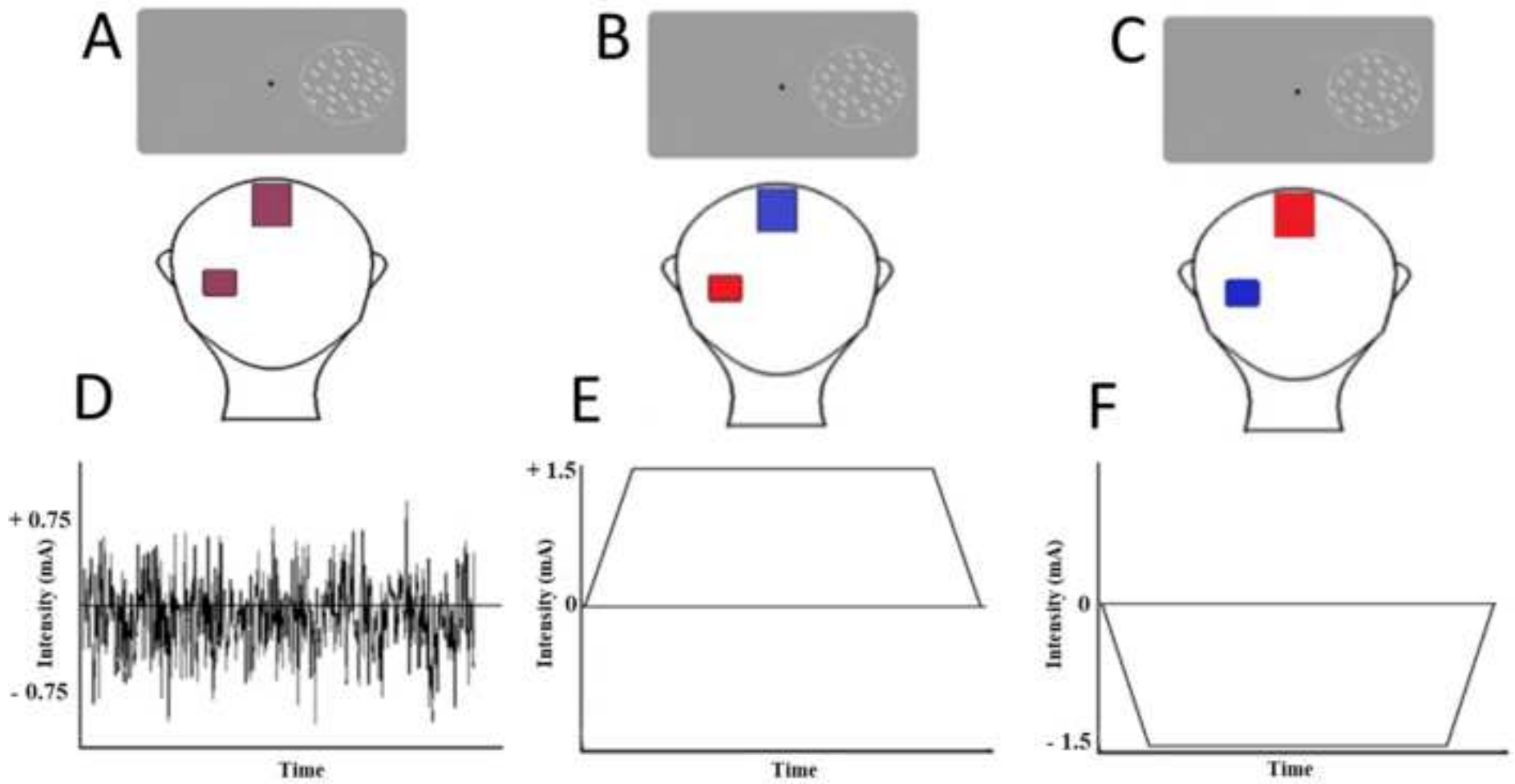

Figure 2

Click here to download high resolution image

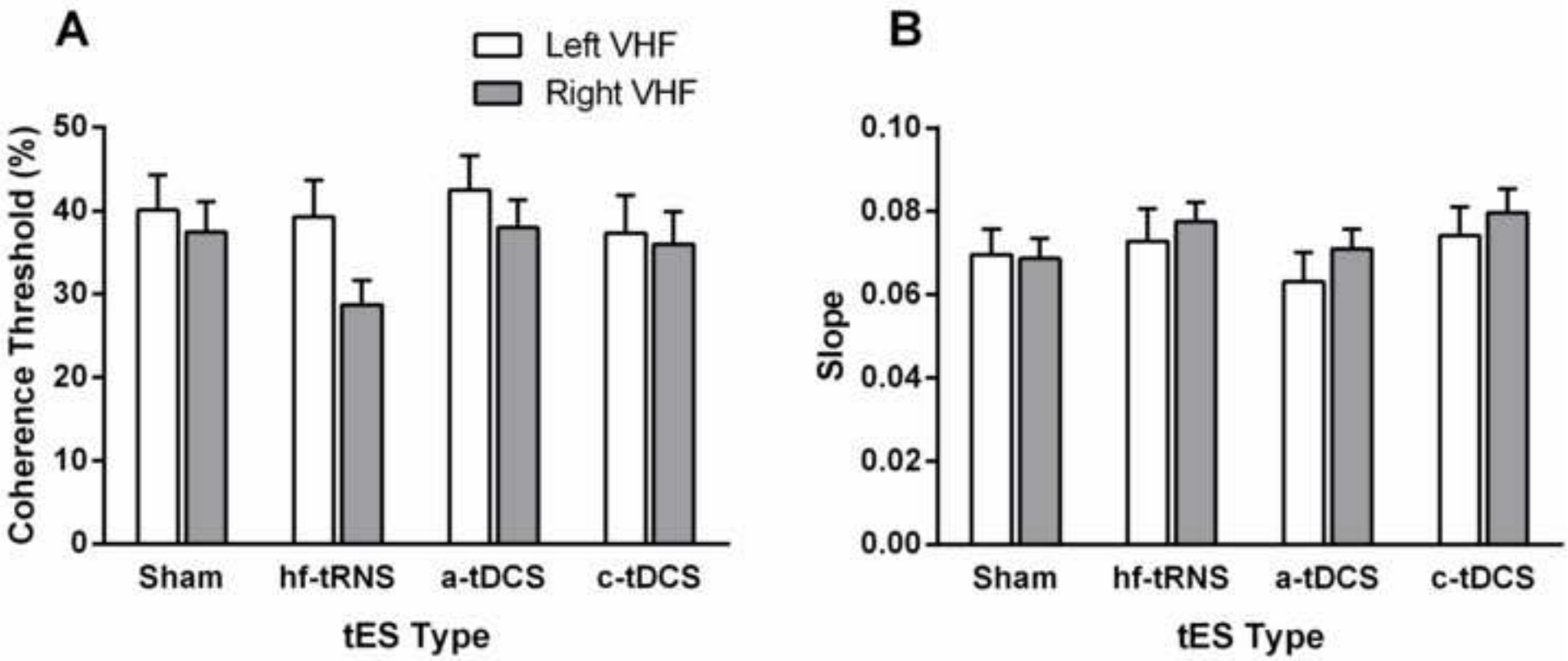

Figure 3

Click here to download high resolution image

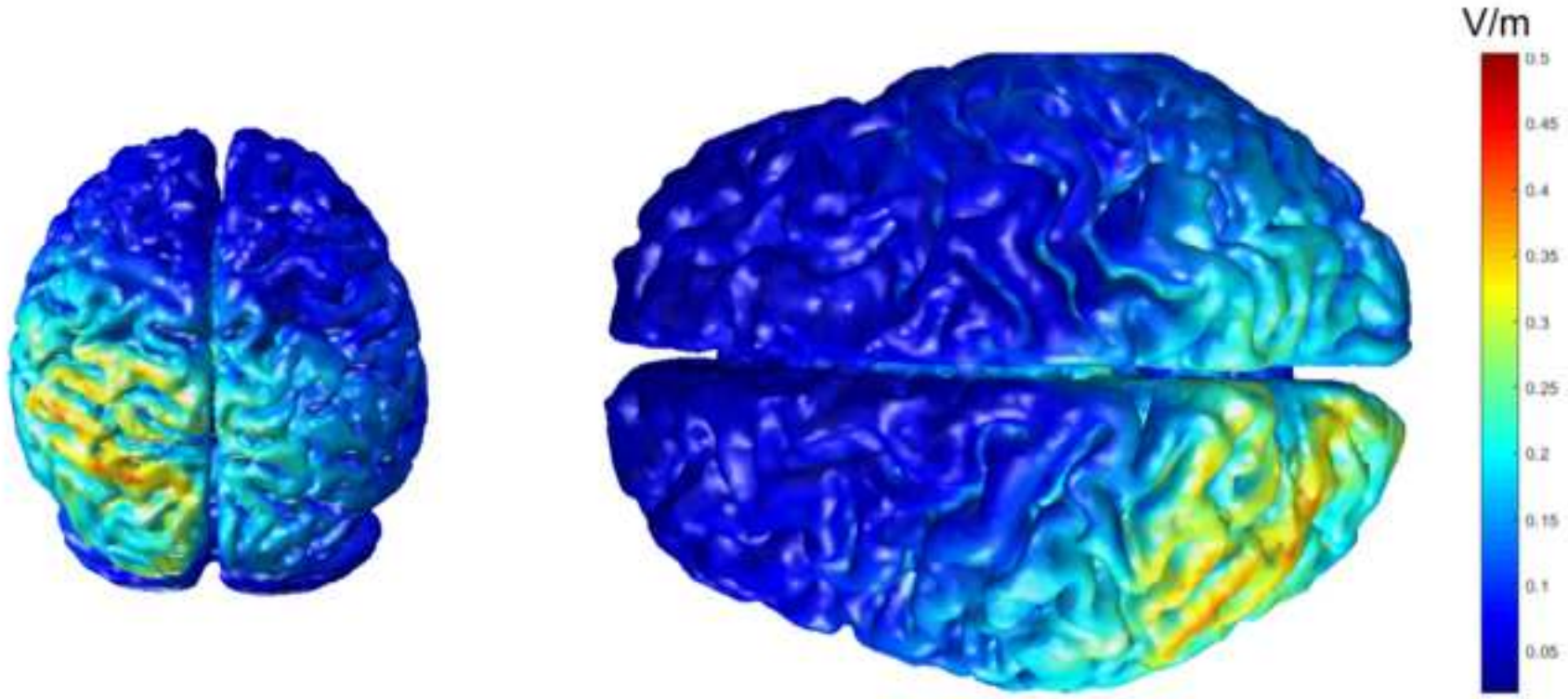

Figure 4
Click here to download high resolution image

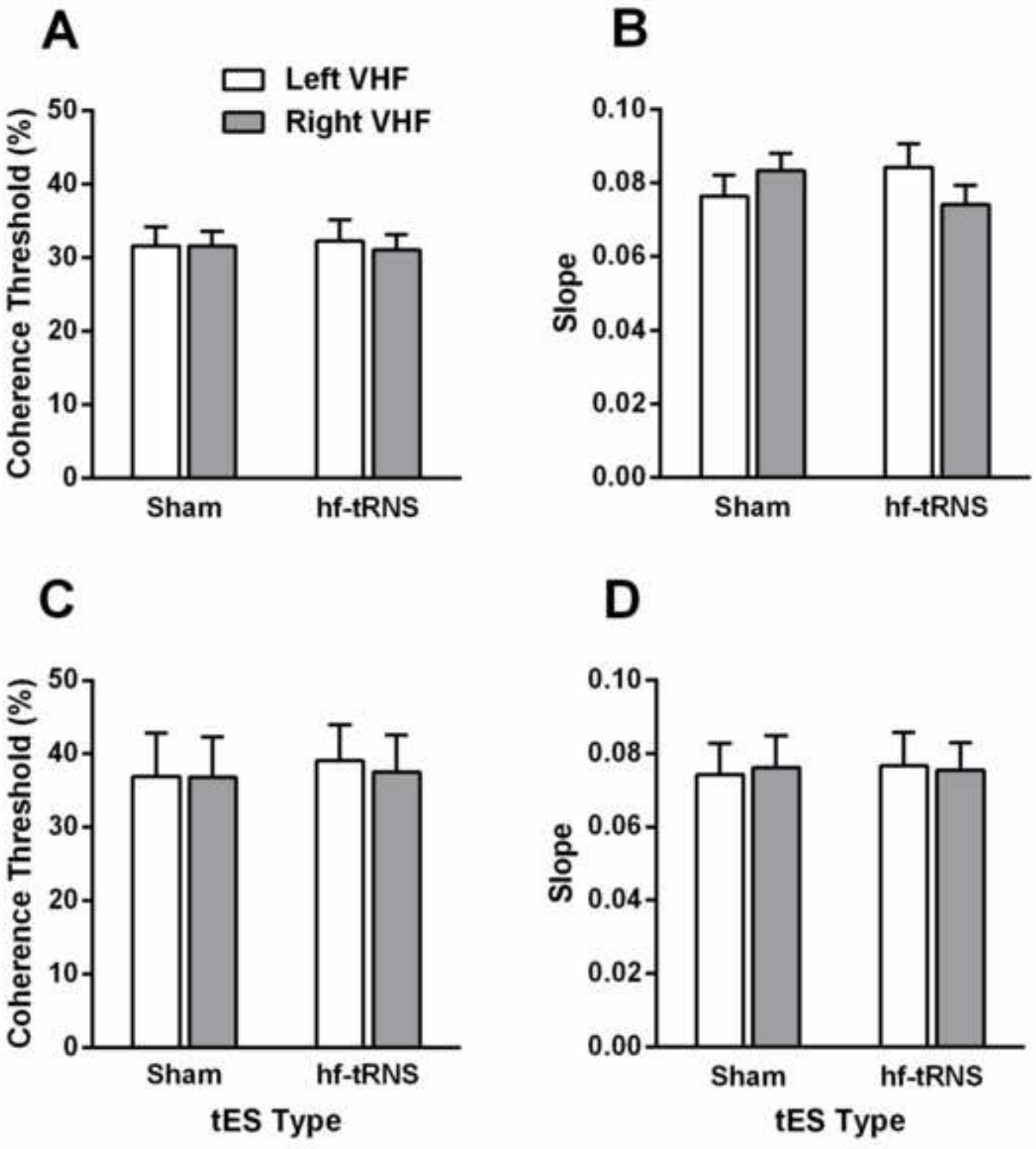

Figure 5
Click here to download high resolution image

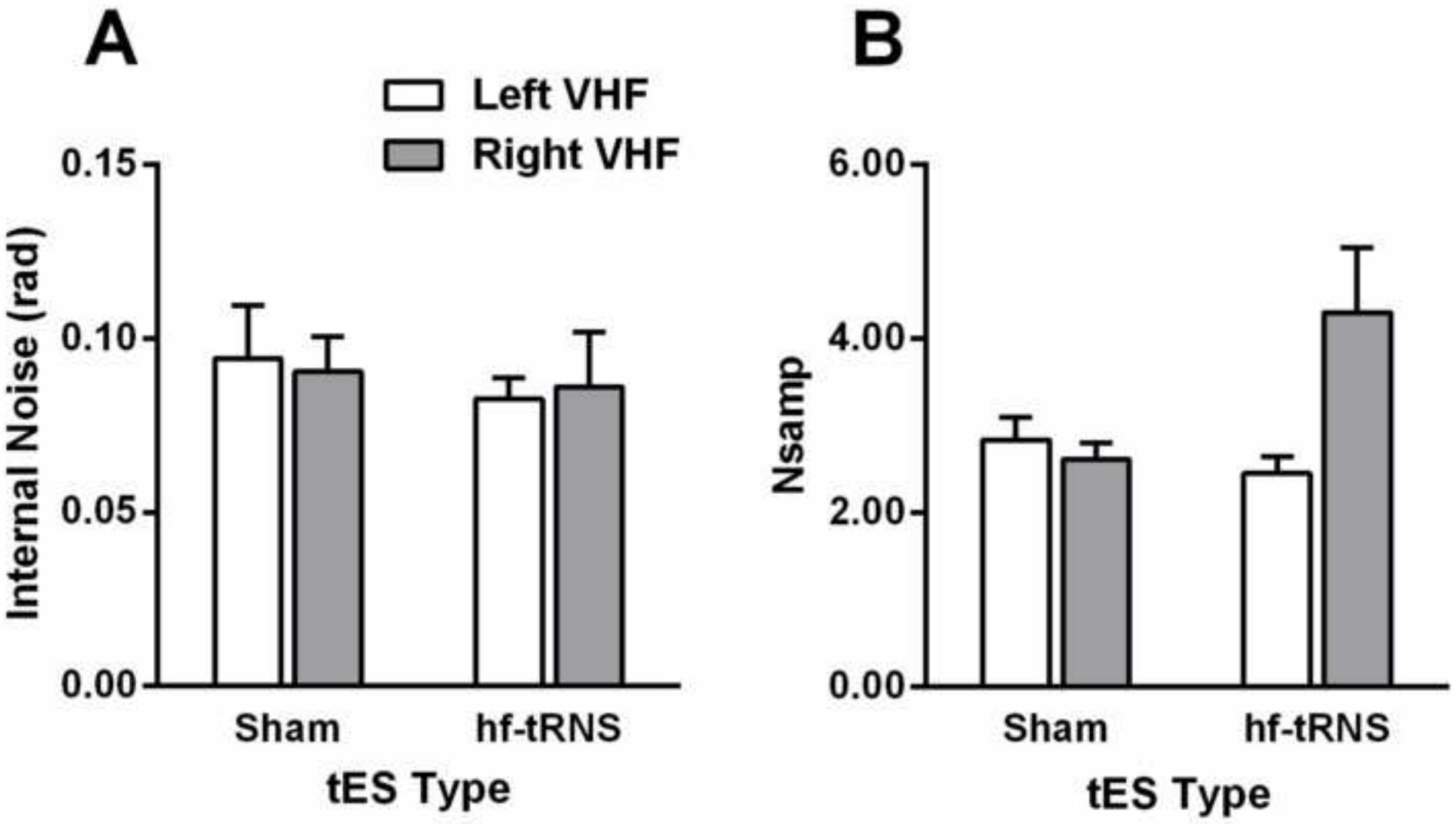

Figure B1

Click here to download high resolution image

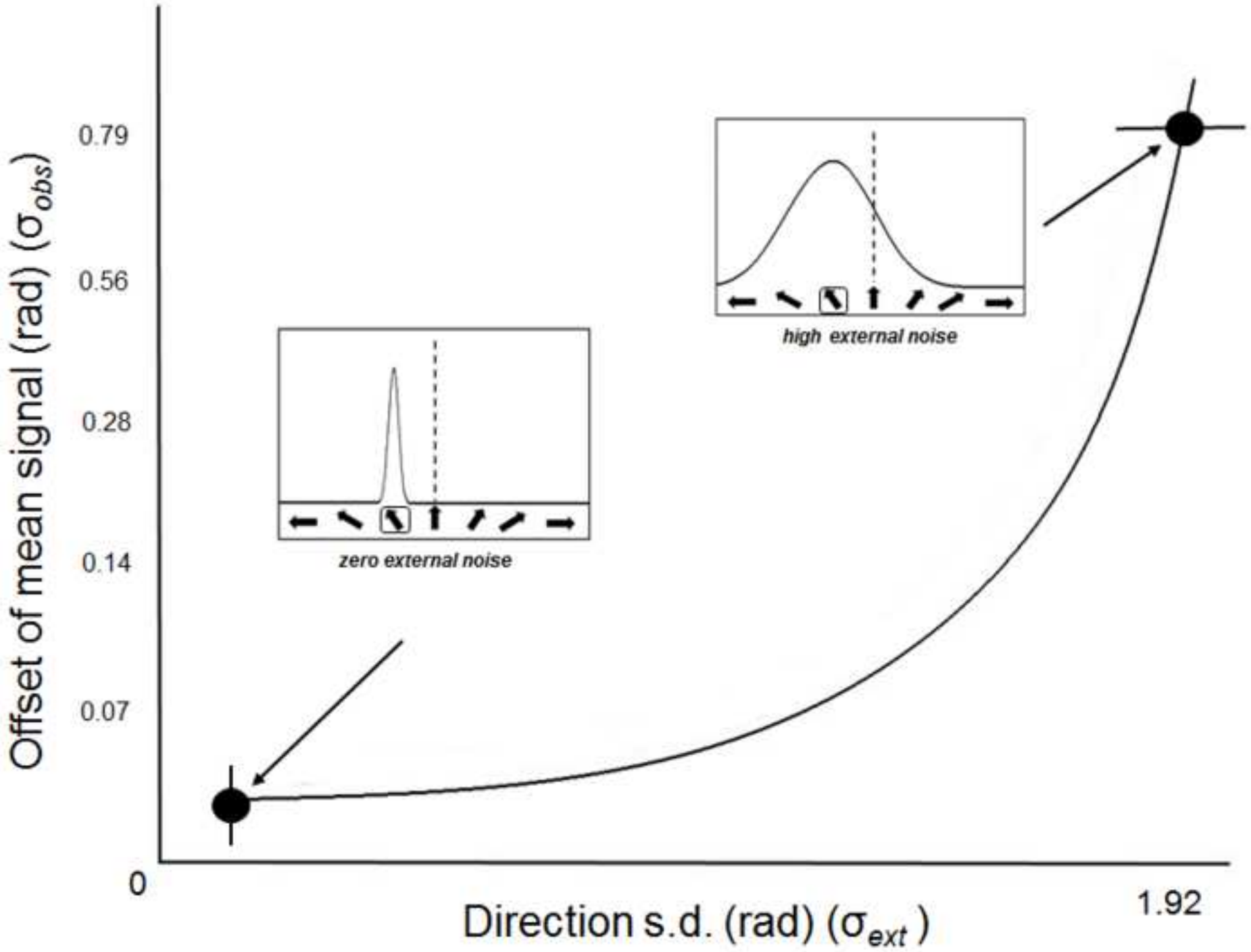

Figure B2

Click here to download high resolution image

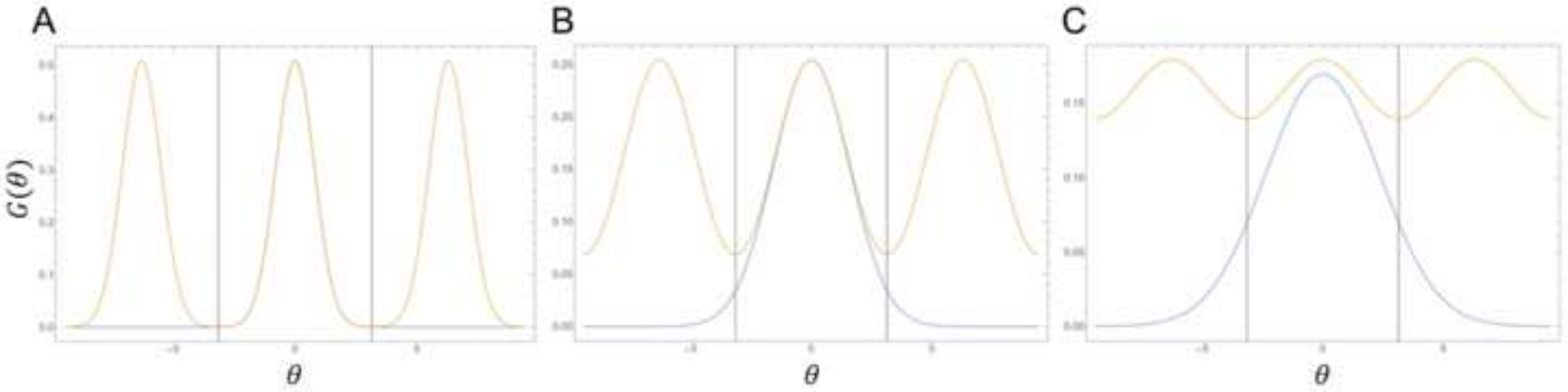

Figure B3
Click here to download high resolution image

Your image file "Figure B3.tiff" cannot be opened and processed. Please see the common list of problems, and suggested resolutions below.

Reason: The image file is corrupt or invalid. Please check and resubmit.

Other Common Problems When Creating a PDF from an image file

You will need to convert your image file to another format or fix the current image, then re-submit it.

Table 1

Coefficient	Estimate (β)	Std. Err (SE)	Wald	p-value
Intercept	0.09145	0.01002	83.33	<0.001
Stimulation Type	-0.00282	0.01815	0.02	0.88
Visual hemi-field	0.004235	0.01782	0.06	0.81
Stimulation type * Visual hemi-field	-0.00932	0.022612	0.17	0.68

Table 2

Coefficient	Estimate (β)	Std. Err (SE)	Wald	p-value
Intercept	2.609	0.181	206.74	<0.001*
Stimulation Type	1.719	0.695	6.12	0.013*
Visual hemi-field	0.231	0.314	0.54	0.48
Stimulation type * Visual hemi-field	-2.126	0.613	12.94	<0.001*

***Conflict / Declaration of Interest form**

Click here to download Conflict / Declaration of Interest form: declaration of interest.docx